[American Journal of Science, Vol. 318, March, 2018, P. 300–334, DOI 10.2475/03.2018.02]

HIGH-RESOLUTION MAGNETOSTRATIGRAPHY OF THE UPPER NACIMIENTO FORMATION, SAN JUAN BASIN, NEW MEXICO, USA: IMPLICATIONS FOR BASIN EVOLUTION AND MAMMALIAN TURNOVER

CAITLIN LESLIE*,†, DANIEL PEPPE*, THOMAS WILLIAMSON**, DARIO BILARDELLO***, MATTHEW HEIZLER§, ROSS SECORD§§, and TYLER LEGGETT*

ABSTRACT. Lower Paleocene deposits in the San Juan Basin document one of the best records of mammalian change and turnover following the Cretaceous-Paleogene mass extinction and is the type area for the Puercan (Pu) and Torrejonian (To) North America Land Mammal age (NALMA). One of the largest mammalian turnover events in the early Paleocene occurs between the Torrejonian 2 (To2) and Torrejonian 3 (To3) NALMA interval zones. The Nacimiento Formation contains the only deposits in North America where the To2-To3 mammalian turnover can be constrained; however, the precise age and duration of the turnover is poorly understood due to the lack of a precise chronostratigraphic framework. We analyzed paleomagnetic samples, produced a $^{40}Ar/^{39}Ar$ detrital sanidine age, and developed a detailed lithostratigraphy for four sections of the upper Nacimiento Formation in the San Juan Basin, New Mexico (Kutz Canyon, Escavada Wash, Torreon West and East) to constrain the age and duration of the deposits and the To2-To3 turnover. The polarity stratigraphy for the four sections can be correlated to chrons C27r-C26r of the geomagnetic polarity time scale (GPTS). Using the local polarity stratigraphy for each section, we calculated a mean sediment accumulation rate and developed a precise age model, which allows us to determine the age of important late Torrejonian mammalian localities. Using the assigned ages, we estimate the To2-To3 turnover was relatively rapid and occurred over ~120 kyr (−60/+50 kyr) between 62.59 and 62.47 Ma. This rapid duration of mammalian turnover suggests that it was driven by external forcing factors, such as environmental change driven by the progradation of the distributive fluvial system across the basin and/or changes in regional or global climate. Additionally, comparisons of the mean sediment accumulation rates among the sections that span from the basin margin to the basin center indicate that sediment accumulation rates equalized across the basin from the end of C27r through the start of C26r, suggesting an accommodation minimum in the basin associated with the progradation of a distributive fluvial system into the basin. This accommodation minimum also likely led to the long hiatus of deposition between the Paleocene Nacimiento Formation and the overlying Eocene San Jose Formation.

Keywords: Paleocene, paleomagnetism, rock magnetism, basin evolution, mammalian evolution, North American Land Mammal age, Torrejonian

INTRODUCTION

The Nacimiento Formation outcrops in the San Juan Basin of northwestern New Mexico (fig. 1) and is composed primarily of terrestrial fluvial rocks. The Nacimiento Formation contains one of the most continuous records of lower Paleocene terrestrial evolution in North America and documents the early Paleocene radiation of mammals

* Terrestrial Paleoclimatology Research Group, Department of Geosciences, Baylor University, One Bear Place #97354, Waco, Texas 76706, USA
** New Mexico Museum of Natural History and Science, Albuquerque, New Mexico 87104, USA
*** Institute for Rock Magnetism, University of Minnesota, Minneapolis, Minnesota 55455, USA
§ New Mexico Bureau of Geology, New Mexico Tech, Socorro, New Mexico 87801, USA
§§ University of Nebraska-Lincoln, Department of Earth and Atmospheric Sciences, Lincoln, Nebraska 68588, USA
† Corresponding author: Caitlin_Leslie@baylor.edu; CaitlinELeslie@gmail.com

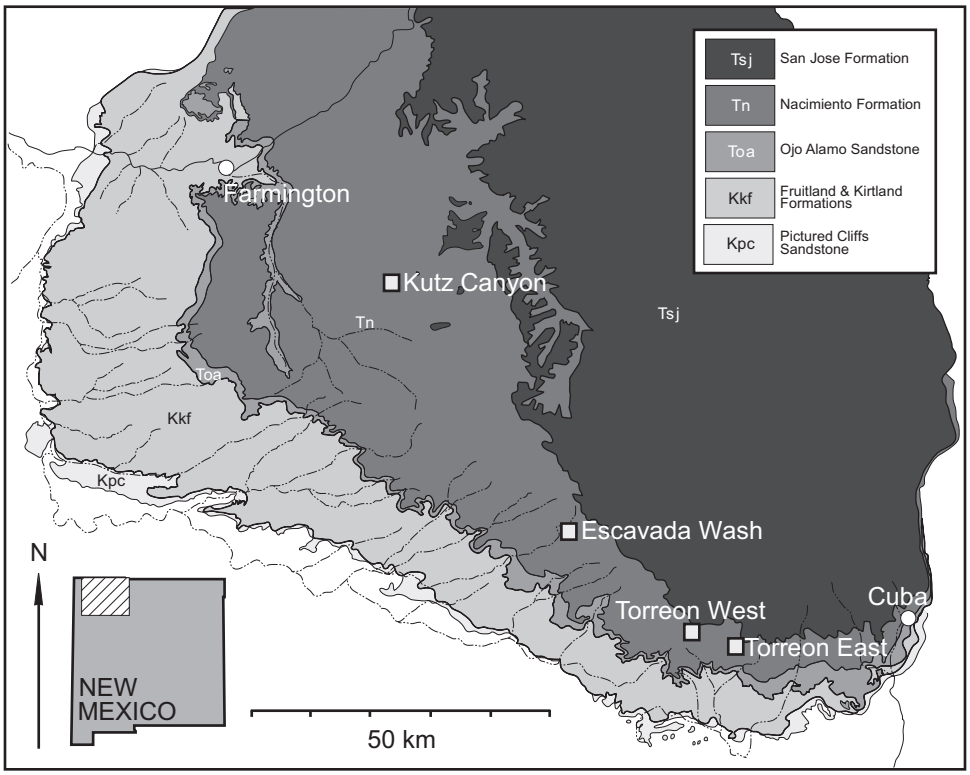

Fig. 1. Geologic map of the San Juan Basin, New Mexico showing the Cretaceous through Eocene sediments and the locations of the four sections collected in this study, Kutz Canyon, Escavada Wash, Torreon West, and Torreon East, indicated by white squares (modified from Williamson and others, 2008).

when mammals rapidly diversified following the Cretaceous-Paleogene (K-Pg) mass extinction (Williamson, 1996). The San Juan Basin is the "type" area for the early Paleocene Puercan (Pu) and Torrejonian (To) North American Land Mammal age interval zones (NALMAs) that were first defined based on mammalian assemblages from the Nacimiento Formation (Wood and others, 1941). These mammal assemblages continue to be critical for the characterization and definition of early Paleocene NALMAs and their subdivisions (Archibald and others, 1987; Lofgren and others, 2004).

Matthew (1937) provided the first comprehensive review of the long history of fossil mammalian collections from the Nacimiento Formation. Williamson (1996) documented two significant intervals of mammalian turnover within the formation, between Puercan 2 (Pu2) and Puercan 3 (Pu3) and between Torrejonian 2 (To2) and Torrejonian 3 (To3) that exhibit high rates of turnover. However, the precise timing of these turnovers and their contemporaneous nature across the basin is uncertain. The Nacimiento Formation is the only continuous record of the To2-To3 turnover interval in North America, therefore a more precise geochronologic framework is needed to better evaluate biotic change through this critical interval of time.

Magnetostratigraphy has been used to develop a chronostratigraphic framework for the Nacimiento Formation with the aim of providing a geochronologic framework for study of vertebrate evolution and evaluating the timing of mammalian faunal change for much of the early Paleocene (Butler and others, 1977; Taylor, ms, 1977;

Butler and Taylor, 1978; Lindsay and others, 1978, 1981; Taylor and Butler, 1980; Butler and Lindsay, 1985). However, a high-resolution age model in conjunction with detailed stratigraphy is still lacking for portions of the formation, and particularly for the To2-To3 interval.

In this study, we focus on developing a high-resolution age model for mammalian turnover between the To2 and To3 interval zones across the San Juan Basin. We develop a detailed lithostratigraphy in conjunction with the Torrejonian mammal localities and determine the magnetostratigraphy of four sections across the basin that span the To2-To3 boundary. These sections are: Kutz Canyon, Escavada Wash, Torreon West, and Torreon East (fig. 1). We then correlate the polarity stratigraphy of each section to the global geomagnetic polarity time scale (GPTS) (Ogg, 2012) with the help of a $^{40}Ar/^{39}Ar$ detrital sanidine age to constrain the timing and duration of sediment deposition in each section. Using calculated sediment accumulation rates, we assign an age to each fossil locality within the sections to correlate the Torrejonian mammal localities across the basin and constrain the age of the To2-To3 mammalian turnover. Finally, we use comparisons of sediment accumulation rates among the four sections to assess the evolution of deposition in the upper Nacimiento Formation.

PREVIOUS WORK

Lithostratigraphy

The San Juan Basin of northwestern New Mexico is a Laramide foreland basin containing Upper Cretaceous through lower Eocene deposits (fig. 1) (Chapin and Cather, 1981). Cather (2004) documents three phases of subsidence in the San Juan basin: an early phase during the late Campanian-early Maastrichtian, a medial phase during the latest Maastrichtian-early Paleocene, and a last phase during the Eocene. The medial phase (~74–67 Ma) allowed for the deposition of the Nacimiento Formation which is composed of alluvial deposits that are subdivided into three members: the Arroyo Chijuillita, the Ojo Encino, and the Escavada members (Williamson and Lucas, 1992; Williamson, 1996). The Ojo Alamo Sandstone underlies the Nacimiento Formation, representing earliest Paleocene deposition in the basin, and the lower Eocene San Jose Formation unconformably overlies the Nacimiento Formation. This study focuses on the Ojo Encino Member of the Nacimiento Formation that contains variegated red and drab paleosols, sheet and channel sandstone units, and three persistent "black" paleosols that we refer to as the "lower black", "middle black", and "upper black". These black beds are useful marker beds as they can be correlated across the basin. The abundant red beds in the Ojo Encino Member distinguish it from the drab colored mudstone and sandstone beds of the underlying Arroyo Chijuillita Member and the high proportion of sandstones and silcretes of the overlying Escavada Member (Williamson and Lucas, 1992; Williamson, 1996; Davis and others, 2016).

The four sections investigated in this study are spread along a northwest-southeast transect through the basin and span from basin center to basin margin (fig. 1). Kutz Canyon, the northernmost section, is near the center of the basin, Escavada Wash is near the basin margin approximately 48 km southeast of Kutz Canyon, and Torreon West and East, the southernmost sections, are approximately 32 km southeast of Escavada Wash near the basin margin. Torreon West and East are separated by about 10 km. Taylor (ms, 1977) produced the first stratigraphic sections, collected paleomagnetic samples, and documented the stratigraphic position of fossil mammal localities for Torreon West, Torreon East, and the Big Pocket fossil locality in Kutz Canyon. In the measured sections, lithologies were generalized and lumped into siltstone, sandstone, volcanic ash, and coal intervals. Taylor (ms, 1977) also identified lower, middle, and upper "carbonaceous" clay beds that outcrop as distinct black intervals, referred to the lower, middle, and upper blacks in this paper. Williamson (1996) subsequently

produced more detailed measured sections for Torreon West, Torreon East, Kutz Canyon, and Escavada Wash by documenting pedogenic features and reporting Munsell colors for mudstones. However, his sections are not tied directly to magnetostratigraphic sections, and thus are not well constrained geochronologically.

Paleomagnetism and Rock Magnetism

Taylor and Butler (1980) constructed the magnetic polarity stratigraphy of a 185 m section at Torreon West, a 62 m section at Torreon East, and a 420 m section at Kutz Canyon. The *Deltatherium* mammalian zone (equivalent to Torrejonian 2, *sensu* Lofgren and others, 2004) was recognized at all three sections and the "*Pantolambda* mammalian zone" (*sensu* Osborn, 1929, see below; equivalent to Torrejonian 3, *sensu* Lofgren and others, 2004) at Torreon West and Kutz Canyon. The two zones were estimated to be separated by about 500 kyr. The section at Kutz Canyon, measured at the Big Pocket fossil locality, includes approximately 100 m of strata below the *Deltatherium* zone. The paleomagnetic sample spacing for all sections was approximately 3 meters. The Torreon West, Torreon East, and upper portion of the Kutz Canyon sections were correlated to C26r to C25r based on previous work correlating the Upper Cretaceous through middle Paleocene San Juan Basin deposits to the geomagnetic polarity time scale (GPTS) (Taylor, ms, 1977; Lindsay and others, 1978). Following the work of Taylor and Butler (1980), Butler and Lindsay (1985) recognized magnetic overprinting in the lower part of the section and revised correlation of the polarity zones to C27r to C26r rather than C26r to C25r. Despite the numerous mammalian localities identified at Escavada Wash, a polarity stratigraphy has not been constructed until now.

Taylor and Butler (1980) identified the persistent black mudstones at Torreon West and East that function as excellent marker beds to reference the stratigraphic position of reversals in each section. The C27r-C27n reversal was reported near the base of the middle black at Torreon West and near the top of the middle black at Torreon East and the C26r-C27n reversal was reported at the base of the upper black at Torreon West and 9 m below the base at Torreon East. These findings suggest that the blacks are diachronous despite the proximity of the two sections.

A rock magnetic study of the San Juan Basin deposits was also conducted by Butler and Lindsay (1985) who analyzed magnetic separates from nine stratigraphic levels through Upper Cretaceous to middle Paleocene deposits; however, the exact sample locations are unclear and therefore it is unknown whether any sample overlap exists with the new sections presented here. Butler and Lindsay (1985) determined that titanohematite of intermediate composition was the dominant magnetic mineral based on microprobe and X-ray analyses, supported by Curie temperatures ranging from 180 to 300 °C. These findings indicate the sediments were likely sourced from volcanic rocks of the San Juan Mountain region to the north, based on the presence of titanohematite. Kodama (1997) measured the anisotropy of remanence on samples of the Nacimiento Formation collected from Kutz Canyon to conduct an inclination shallowing correction and found support for a primary detrital magnetization for the formation.

Mammalian Biostratigraphy

Mammalian interval zones in the San Juan Basin have a long and complicated history. Sinclair and Granger (1914) established the presence of two zones of distinct mammalian assemblages at Torreon Wash, the *Deltatherium* and *Pantolambda* zones, which are separated by approximately 30 m of non-fossiliferous deposits. Osborn (1929) treated the two zones as separate life zones representing different ages and formally named and characterized the *Deltatherium* zone by the presence of *Deltatherium fundaminis*, *Mioclaenus turgidus*, and *Haploconus angustus* and the *Pantolambda* zone by

the presence *of Pantolambda cavirictum* and *Arctocyon ferox*. However, others considered these two zones to be a facies effect, sampling bias, or inaccurate due to the presence of the same species in both zones (Granger, 1917; Matthew, 1937; Wilson, 1956; Russell, 1967). Using magnetostratigraphy, Taylor and Butler (1980) demonstrated that the *Deltatherium* and *Pantolambda* zones represent different ages at Torreon Wash. Taylor (ms, 1984) renamed the *Deltatherium* and *Pantolambda* zones *Deltatherium – Tetraclaenodon* (D-T) and *Pantolambda bathmodon – Mixodectes pungens* (P-M) after the discovery of *Pantolambda cavirictum* in other localities in the basin within the upper portion of the "*Deltatherium* zone".

Archibald and others (1987) updated the Paleocene NALMAs and divided the Torrejonian into three zones, To1-To3, using the San Juan Basin mammalian assemblages to establish the To2 and To3 mammal ages. The *Deltatherium* and *Pantolambda* zones established by Sinclair and Granger (1914) are equivalent to To2 and To3, respectively, of Archibald and others (1987). Archibald and others (1987) defined To2 as the *Tetraclaenodon-Pantolambda* zone and To3 as the *Pantolambda-Plesiadapis praecursor* zone, placing the boundary between the two zones within the upper part of the *Deltatherium* zone of Sinclair and Granger (1914). Williamson (1996) further subdivided the To2 and To3 interval into five biostratigraphic zones within the San Juan Basin: P-E zone (lowest occurrence of *Protoselene opisthacus* and lowest occurrence of *Ellipsodon granger*), E-A zone (lowest occurrence of *Ellipsodon granger* and first occurrence of *Arctocyon ferox*), A-P zone (lowest occurrence of *Arctocyon ferox* and lowest occurrence of *Pantolambda cavirictum*), P-M zone (lowest occurrence of *Pantolambda cavirictum* and first occurrence of *Mixodectes pungens*), and M zone (first and last occurrence of *Mixodectes pungens*). Williamson (1996) defined the A-P zone exclusively from Kutz Canyon and the P-M zone from Torreon West, Kutz Canyon, and two other locations in the basin, Kimbeto and Betonnie-Tsosie washes. The M zone was defined from Torreon East and West and Escavada Wash.

In their revision of Paleocene NALMAs, Lofgren and others (2004) redefined the To2 interval zone as the *Protoselene opisthacus-Mixodectes pungens* interval zone, based primarily on the faunal succession observed at Kutz Canyon and the To3 interval zone as the *Mixodectes pungens-Plesiadapis praecursor* interval zone based primarily on the faunal record at Torreon Wash. With these revisions, To2 is approximately equivalent to the duration of the local San Juan Basin biozones P-E through P-M (Williamson, 1996), and approximately equivalent to the *Deltatherium* zone (Sinclair and Granger, 1914). To3 is nearly equivalent to the duration of the M biozone (Williamson, 1996) and the *Pantolambda* zone (*sensu* Sinclair and Granger, 1914).

Using the Torrejonian zonation of Lofgren and others (2004), there are significant changes in therian mammals across the To2-To3 boundary in the San Juan Basin. The changes observed between the last two San Juan Basin biozones in To2, the A-P and P-M zones, and To3, the M zone are locally considerable (Williamson, 1996). Intense collecting efforts over the last twenty years have resulted in modifications of the San Juan Basin biozones of Williamson (1996), including the movement of several localities from the P-M zone to the older A-P zone (table 1). Despite this extensive collecting, collection biases remain among the fossil zones. For example, the A-P and P-M zones contain few microvertebrate sites, but several are present in the M zone. Additionally, the A-P and P-M zones are generally less fossiliferous and have significantly fewer fossil sites than the M zone.

Despite potential issues with collection biases, there are notable differences between the P-M and M zones in species occurrences and abundance. Several taxa found in the P-M zone, but not the M zone represent medium- to large-bodied taxa that are abundant in P-M zone faunas, making their disappearance across the To2-To3 boundary particularly significant. These are the 'triisodontid' 'condylarth' *Triisodon*

TABLE 1

Selected Mammal Localities and Calculated Ages

Mammal Localities	NALMA interval zone (Lofgren and others, 2004)	San Juan Basin biozone (Williamson, 1996)	Strati-graphic position (m)	Calculated age (Ma)
Kutz Canyon				
Sedimentation rate: 119.9 (-16.3, +18.7) m/myr				
1: L-00400	To2	A-P zone	1-6	62.76-62.71 (-0.04, +0.05)
2: L-06419	To2	A-P zone	1-6	62.76-62.71 (-0.04, +0.05)
3: L-09907, L-09908, L-09909	To2	A-P zone	10	62.68 (-0.00, +0.00)
4: L-08234	To2	P-M zone	16	62.63 (-0.00, +0.01)
Escavada Wash				
Sedimentation rate: 115.7 (-30.3, +34.7) m/myr				
5: L-10453	To2	P-M zone	6.5	62.80 (-0.09, +0.11)
6: L-09187	To2	P-M zone	15.25	62.72 (-0.08, +0.08)
7: L-09985	To2	P-M zone	15.25	62.72 (-0.08, +0.08)
8: L-10554	To2	P-M zone	15.25	62.72 (-0.08, +0.08)
9: L-10350	To2	P-M zone	16.5	62.71 (-0.07, +0.08)
10: L-09981	To3	M zone	59	62.35 (-0.10, +0.05)
11: L-10444	To3	M zone	59	62.35 (-0.10, +0.05)
12: L-10556	To3	M zone	61	62.33 (-0.10, +0.06)
13: L-09982	To3	M zone	62	62.32 (-0.10, +0.06)
14: L-10415	To3	M zone	63	62.31 (-0.11, +0.06)
15: L-10660	To3	M zone	63.25	62.31 (-0.11, +0.06)
16: L-10414	To3	M zone	64.5	62.30 (-0.11, +0.06)
17: L-10403	To3	M zone	65	62.29 (-0.11, +0.06)
18: L-09197	To3	M zone	65.15	62.29 (-0.11, +0.06)
Torreon West				
Sedimentation rate: 119.9 (-10.1, +11.6) m/myr				
19: L-08182	To2	A-P zone	19.75	62.66 (-0.03, +0.04)
20: L-08178	To2	A-P zone	23.25	62.63 (-0.03, +0.03)
21: L-08180	To2	P-M zone	27.5	62.59 (-0.02, +0.03)
22: L-09173	To3	M zone	43	62.46 (-0.02, +0.03)
23: L-08183	To3	M zone	45	62.45 (-0.02, +0.03)
24: L-10500	To3	M zone	48	62.42 (-0.03, +0.03)
25: L-06898	To3	M zone	50.5	62.40 (-0.03, +0.03)
26: L-10490	To3	M zone	55.5	62.36 (-0.03, +0.04)
27: L-07108	To3	M zone	57	62.35 (-0.03, +0.04)
28: L-07582	To3	M zone	57	62.35 (-0.03, +0.04)
29: L-10493	To3	M zone	57.75	62.34 (-0.03, +0.04)
30: L-10494	To3	M zone	57.75	62.34 (-0.03, +0.04)
31: L-10495	To3	M zone	57.75	62.34 (-0.03, +0.04)
32: L-01121	To3	M zone	58.5	62.33 (-0.03, +0.04)
33: L-10534	To3	M zone	59.25	62.33 (-0.04, +0.04)
34: L-10558	To3	M zone	59.25	62.33 (-0.04, +0.04)
35: L-10561	To3	M zone	59.25	62.33 (-0.04, +0.04)
36: L-07848	To3	M zone	59.75	62.32 (-0.04, +0.04)
37: L-08205	To3	M zone	59.75	62.32 (-0.04, +0.04)
38: L-10506	To3	M zone	61.5	62.31 (-0.04, +0.04)
39: L-10535	To3	M zone	61.5	62.31 (-0.04, +0.04)
40: L-10512	To3	M zone	63.5	62.29 (-0.04, +0.04)
41: L-10560	To3	M zone	63.5	62.29 (-0.04, +0.04)
42: L-10505	To3	M zone	66	62.27 (-0.04, +0.04)

TABLE 1
(continued)

Mammal Localities	NALMA interval zone (Lofgren and others, 2004)	San Juan Basin biozone (Williamson, 1996)	Stratigraphic position (m)	Calculated age (Ma)
Torreon East				
Sedimentation rate: 87.0 (-8.0, +9.0) m/myr				
43: L-07725	To2	A-P zone	18.5	62.66 (-0.03, +0.04)
44: L-08227	To2	A-P zone	18.5	62.66 (-0.03, +0.04)
45: L-08228	To2	A-P zone	18.5	62.66 (-0.03, +0.04)
46: L-07583	To2	A-P zone	21.25	62.63 (-0.02, +0.04)
47: L-04954	To2	A-P zone	21.25	62.63 (-0.02, +0.04)
48: L-04950	To2	A-P zone	21.25	62.63 (-0.02, +0.04)
49: L-10013	To3	M zone	35	62.47 (-0.02, +0.03)
50: L-10432	To3	M zone	35	62.47 (-0.02, +0.03)
51: L-09166	To3	M zone	39	62.43 (-0.02, +0.03)
52: L-09167	To3	M zone	39	62.43 (-0.02, +0.03)
53: L-01079	To3	M zone	52	62.28 (-0.04, +0.05)
54: L-09169	To3	M zone	52	62.28 (-0.04, +0.05)
55: L-10454	To3	M zone	52	62.28 (-0.04, +0.05)
56: L-09172	To3	M zone	52	62.28 (-0.04, +0.05)

quivirensis, the periptychid 'condylarth' *Haploconus angustus*, and the enigmatic 'condylarth'? *Deltatherium fundaminis*. The taeniodont *Huerfanodon torrejonius* and the mioclaenid 'condylarth' *Ellipsodon yotankae* are uncommon in the P-M zone and do not appear in the M zone. Considering the difference in collection size and localities between the P-M and M zones, the disappearance of these taxa appears to be significant. Several taxa reported from the M zone, but not from the P-M zone (*Picrodus calgariensis,* the palaeanodont? *Escavadodon zygus,* the hyopsodontid 'condylarth' *Haplaletes* sp., and the arctocyonid 'condylarth' *Colpoclaneus procyonoides*) are rare in the M zone, and thus their absence from the P-M zone could be due to sampling biases between the zones.

In addition to differences in taxonomic occurrences, there are notable differences in the morphology of the mammalian taxa between the P-M and M zones. Several of the changes in mammal taxa between the two zones may reflect anagenic changes within a lineage as they represent two species, usually included within a single genus, distinguished primarily by a significant difference in size, for example: *Swaindelphys johansoni* and *S. encinensis*, *Mixodectes malaris* and *M. pungens* (contra Tsentas, 1981 and Szalay and Lucas, 1996, *M. malaris* is not present in the M. zone), *Anasazia williamsoni* and *Torrejonia wilsoni*, and *Pentacodon inversus* and *P. occultus*. Interestingly, for all these "species pairs", the M zone taxon is larger than the P-M zone taxon.

Although the mammalian turnover between To2 and To3 is well defined, the fossils come from different locations and the exact timing of the To2-To3 turnover is uncertain. This demonstrates the need for a robust age model for the To2-To3 intervals in the Nacimiento Formation to allow for correlations of the San Juan Basin mammalian assemblages to other contemporaneous assemblages across North America and to other continents, and to precisely constrain the age of the To2-To3 turnover. For the purposes of this paper, we use the definition of Lofgren and others (2004) for the To2 and To3 interval zones.

METHODOLOGY

Measured Sections

A total of four sections were measured: a 70 m section at Kutz Canyon, a 87 m section at Escavada Wash, a 79 m section at Torreon West, and a 76 m section at Torreon East (figs. 2 and 3). At Torreon West and Torreon East, the base of the lithostratigraphic and magnetostratigraphic sections was the lower black marker bed. The Escavada Wash section contains multiple middle black marker beds so the section began at the lowest black marker bed present at that locality. Kutz Canyon does not contain the lower or middle black marker beds, so this section was measured from a known late To2 mammal locality (Bab's Basin) to ensure overlap with the other sections.

At each section, the outcrop was trenched to remove weathered material and document the lithologic contacts. The paleosols were described at the centimeter scale. The texture, color, ped structure, and shrink-swell features of each paleosol were documented using the guidelines of Soil Survey Staff (1999). For sandstones, the grain size and relationship to underlying strata was characterized.

The stratigraphic positions of mammal localities that occur within each measured section were documented in the field (figs. 2 and 3). Some mammal localities occur lateral to the measured sections and these localities were placed into each section using measurements from marker beds. Here we recognize A-P zone localities at Torreon West and Torreon East for the first time. Table 1 shows each selected mammal locality (localities that contain multiple taxa and can be precisely placed into the section), the numeric code it has been given for this paper, the associated NALMA interval zone, San Juan Basin biozone, and stratigraphic position.

Paleomagnetism

Four paleomagnetic block samples were collected from paleosols, mudstone, and fine grained sandstone beds at ~1 m intervals (0.25 m minimum and 7 m maximum sample spacing) in each section, defining a study site. Lithologies coarser than fine grained sandstones were avoided. Site spacing was primarily dictated by stratigraphic exposure and lithology. When sampling, a flat face was shaved onto the samples *in situ* using a hand rasp and its orientation was measured using a Brunton Pocket Transit Compass. In the laboratory, the samples were cut into approximately 4 cm^3 cubes using a diamond-bit saw. Each sample yielded one cubic specimen.

At Kutz Canyon and Escavada Wash, the entire sections spanning from late To2 through To3 strata were sampled. A total of 48 sites were sampled at Kutz Canyon and 50 sites at Escavada Wash. At Torreon West and East, the position of reversals had been reported by Taylor and Butler (1980) for the entire late To2-To3 succession. Consequently, full sections were not sampled but rather the deposits surrounding the approximate reversal positions were densely sampled to better constrain each reversal. A total of 38 sites were sampled at Torreon West and 44 sites at Torreon East.

Specimens were measured at Baylor University using a 2G Enterprises (Mountain View, California) cryogenic DC-SQuID magnetometer located in a 2-layer magnetostatic shielded room with a background field typically less than 300 nT. All specimens were demagnetized using a thermal demagnetization strategy. Rock magnetic analyses determined the magnetic carriers in the samples had relatively low unblocking temperatures (see below), therefore thermal demagnetization steps were performed in 25° increments up to the maximum unblocking temperature or until the magnetizations became erratic and unstable, ranging between 225° to 400 °C. To minimize oxidation reactions, thermal demagnetization was performed using a nitrogen atmosphere using ASC (Carlsbad, California) controlled atmosphere thermal demagnetizer.

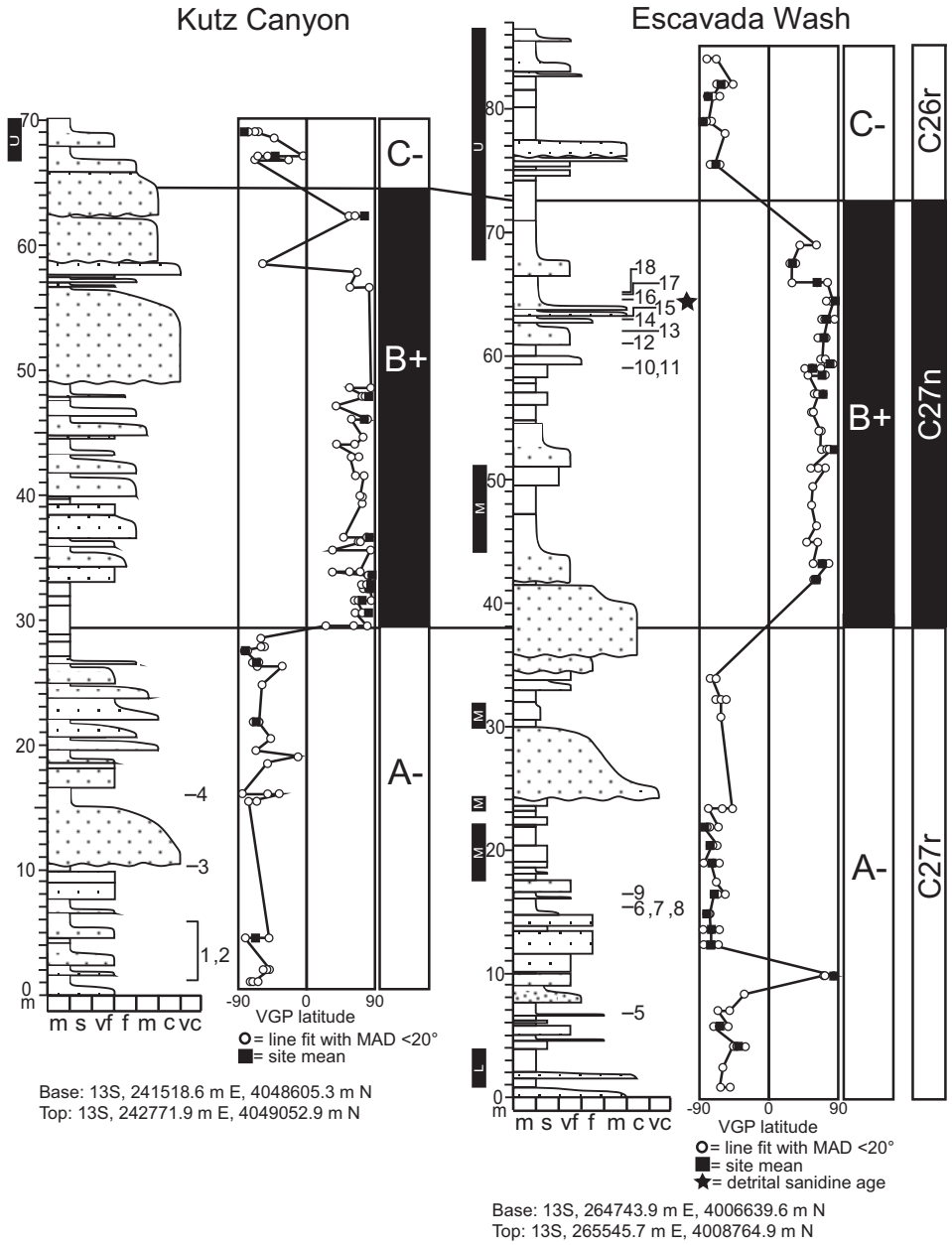

Fig. 2. Measured sections with fossil localities, VGP latitude, and interpreted polarity zonations for the Kutz Canyon and Escavada Wash sections. Note the presence of the black beds highlighted and labeled L (lower), M (middle) and U (upper). The base of the B+ magnetozone is used as the datum. Fossil localities 1–4 from Kutz Canyon and 5–18 from Escavada Wash are described in table 1. Section base and top UTM coordinates shown, NAD27 datum.

Principal-component analysis (PCA) was used to isolate the characteristic remanence for each demagnetized specimen (Kirschvink, 1980). A best-fit line was calculated from at least three demagnetization steps that trended toward the origin and had

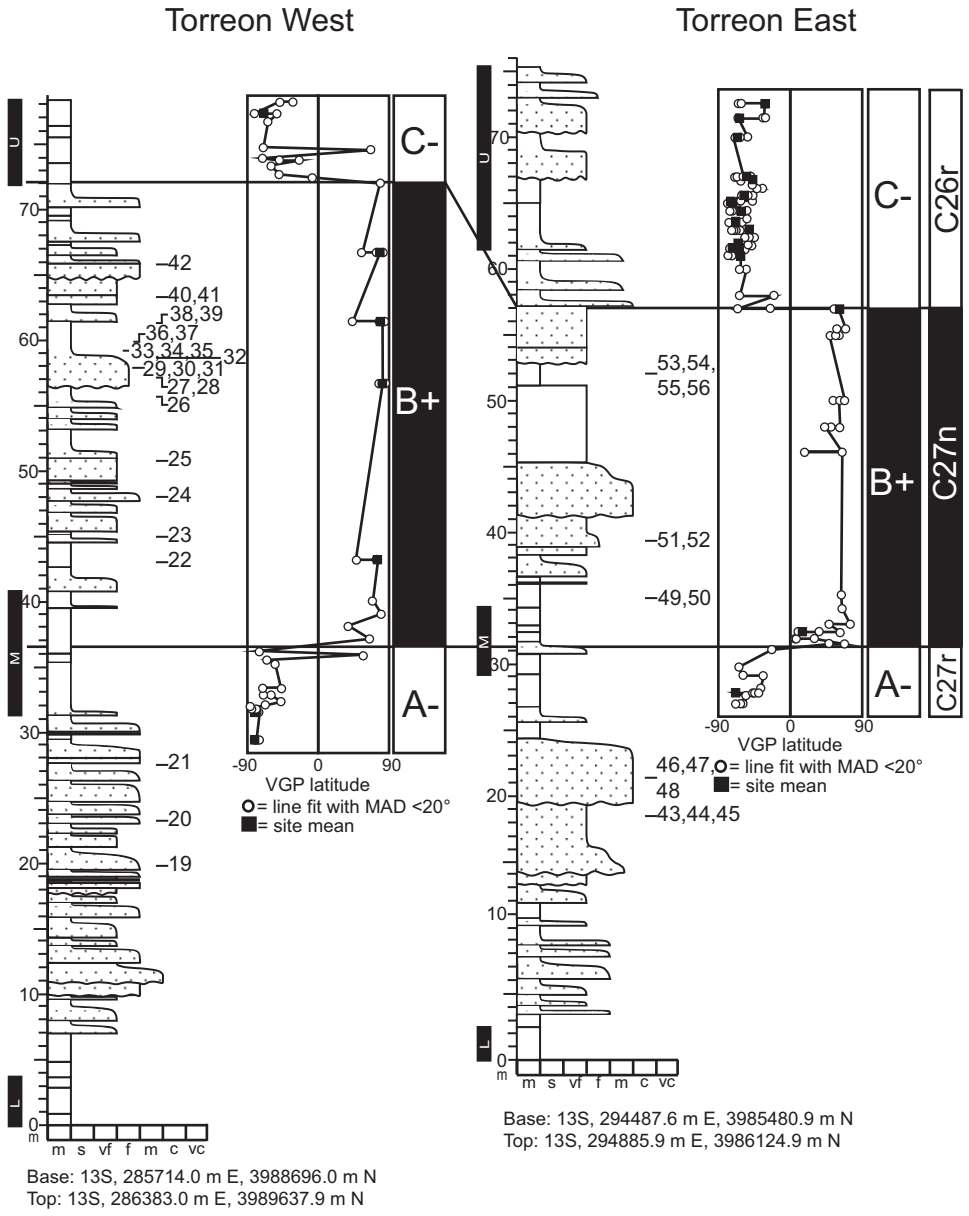

Fig. 3. Measured sections with fossil localities, VGP latitude, and interpreted polarity zonations for the Torreon West and Torreon East sections. Note the presence of the black beds highlighted and labeled L (lower), M (middle) and U (upper). The base of the B+ magnetozone is used as the datum. Fossil localities 19–42 from Torreon West and 43–56 from Torreon East are described in table 1. Section base and top UTM coordinates shown, NAD27 datum.

a maximum angle of deviation (MAD) <20° (Appendix 1). Data from specimens that had erratic demagnetization behaviors were excluded from further analysis. A site mean direction was calculated for all sites with three specimens with statistically significant directions using Fisher statistics (Appendix 2) (Fisher, 1953). If site means

had a 95 percent confidence circle (α_{95}) >35°, which exceeds cut-off values based on the randomness criteria of Watson (1956), they were not used. Reversal boundaries were placed at the stratigraphic midpoints between samples of opposing polarity. The local polarity stratigraphy was then correlated to the geomagnetic polarity time scale (GPTS) (Ogg, 2012). The polarity stratigraphy of the Torreon West and East deposits coarsely resolved by Taylor and Butler (1980) determined the base and top of each section was reversed, therefore the deposits below and above the sampling intervals in this study were interpreted to be reversed.

Rock Magnetism

Rock magnetic analyses were performed at the Institute for Rock Magnetism at the University of Minnesota. To characterize the full suite of magnetic mineralogies present within the study interval, representative samples were chosen that captured the range of lithologies present. The lithologies were categorized into the following categories: black slickensided paleosols, red calcareous paleosols, brown to gray slickensided paleosols, drab-colored slickensided paleosols, and silty weakly-developed paleosols. Saturation magnetization was measured on a MicroMag Princeton Measurements Corporation (Princeton, New Jersey) vibrating sample magnetometer (VSM) on 11 specimens at temperatures ranging from 30°C to 600 °C.

A Quantum Design (San Diego, California) Magnetic Properties Measurement System (MPMS) was used for low-temperature remanence measurements on 18 specimens. The protocol included field-cooled (FC) remanence, zero-field-cooled (ZFC) low-temperature saturation isothermal remanent magnetization (LTSIRM), and room temperature saturation isothermal remanent magnetization (RTSIRM). The method involves applying a sustained DC field of 2.5 T as a specimen is cooled from 300 K to 20 K (FC) and its magnetic remanence is measured upon warming back to room temperature (300 K). Subsequently the specimen is cooled to 20 K with no applied field (ZFC) and a 2.5 T LTSIRM is applied. The magnetic remanence is measured while the specimen warms back to 300 K. A 2.5 T room temperature SIRM (RTSIRM) is then applied at 300K and the magnetic remanence is measured upon cooling to 20 K and warming back to room temperature.

An additional goethite test was performed on four specimens to determine whether goethite was present. The method, similar to that of Guyodo and others (2006), involves heating a sample up to 400 K and then applying a thermal remnant magnetization (TRM) as the sample cools from 400 to 300 K, magnetizing any goethite through its Néel temperature. The applied field is then turned off and the remanence is measured as the specimen is cooled to 20 K and warmed back up to 300 K, allowing the specimens to cycle through the magnetite structural phase transition temperature of ~120 K (the Verwey transition, for example Dunlop and Ozdemir, 1997) resulting in loss of remanence if any magnetite is present. The specimen is then heated to 400 K again in zero field, demagnetizing goethite through its Néel ordering temperature. Remanence is measured while the sample cools to 20 K and warms to 300 K to determine which, if any, magnetic phases remain after the contribution of goethite is removed.

A triaxial-IRM Lowrie test was performed at Baylor University on 11 samples to determine the primary magnetic carrier on mixed mineralogy samples (Lowrie, 1990). 11 cubic specimens were imparted with a 1T, 300 mT, and 100 mT field along the X, Y, and Z axes respectively with an ASC pulse magnetizer. Samples were thermally demagnetized in 50 °C increments from 100 to 650 °C in an ASC controlled atmosphere thermal demagnetizer. Samples were measured using the 2G cryogenic DC-SQuID magnetometer.

Detrital Sanidine Dating

One sample, H16-SJ-11, was collected from a sandstone body at 64 m in Escavada Wash (fig. 2). Processing and mineral separation was done at the New Mexico Geochronology Research Laboratory (NMGRL). Sample separation included: crushing & grinding the rock sample, cleaning with H_2O and 5 percent HF acid, and sieving grain size between 40 and 80 mesh. Magnetic and heavy liquid density separation was used to concentrate the K-feldspar grains. Sanidine was hand-picked from the bulk K-feldspar separate based on optical properties indicative of sanidine as viewed while immersed in wintergreen oil under a polarizing binocular microscope. Approximately 100 grains were selected and then washed in acetone to remove the wintergreen oil.

The crystals were irradiated at the TRIGA reactor in Denver, Colorado, for 8 hours in the NM-291 package along with Fish Canyon Sanidine interlaboratory standard FC-2 with an assigned age of 28.201 Ma (Kuiper and others, 2008). Ages are calculated with a total ^{40}K decay constant of 5.463e-10 /a (Appendix 3) (Min and others, 2000).

After irradiation, six crystals of FC-2 from each of 8 monitor holes from a 24-hole irradiation tray, along with 89 sample crystals were loaded into a copper tray, evacuated and baked at 140 °C for 2 hours. Sample crystals were fused with a CO_2 laser and the extracted gas was cleaned with a NP 10 getter operated at 1.6 A for 30 seconds. The gas was analyzed for argon isotopes using an ARGUS VI multicollector mass spectrometer equipped with five Faraday cups, and one ion counting multiplier (CDD). The configuration had ^{40}Ar, ^{39}Ar, ^{38}Ar, ^{37}Ar and ^{36}Ar on the H1, AX, L1, L2, and CDD detectors, respectively. H1, AX and L2 utilized Faraday detectors equipped with 1×10^{13} Ohm resistors whereas L1 had a Faraday with a 1×10^{14} Ohm resistor. The CDD is an ion counting detector with a dead time of 14 nS. All data acquisition was accomplished with NM Tech Pychron software and data reduction used Mass Spec (v. 7.875) written by Al Deino at the Berkeley Geochronology Laboratory. Extraction line blank plus mass spectrometer background values are averages of numerous measurements interspersed with the unknown measurements. These values are 3±12 percent, 0.16±12 percent, 0.05±11 percent, 0.3±4 percent, 0.03±2.5 percent, $\times10^{-17}$ moles from masses 40, 39, 38, 37, and 36, respectively.

The minimum age population is defined by choosing the youngest dates that form a near Gaussian distribution as defined by the MSWD value of the distribution. The minimum age is the inverse variance weighted mean of the selected crystals and the error is the square root of the sum of $1/\sigma^2$ values. The error is also multiplied by the square root of the MSWD for MSWD greater than 1. J-error (0.03%) is included for the weighted mean age error and all errors are reported at 1σ.

RESULTS

Magnetostratigraphy

One hundred and forty-four samples were analyzed from 48 sampling horizons from Kutz Canyon, 150 samples from 50 sampling horizons from Escavada Wash, 114 samples from 38 sampling horizons from Torreon West, and 132 samples from 44 sampling horizons from Torreon East. The demagnetization trajectory of most specimens trended towards the origin after a few steps and were fully demagnetized by 200° to 400 °C (figs. 4A, 4B, and 4C). All specimens with coherent demagnetization trajectories and stable endpoints were characterized by line fits. In total, reliable paleomagnetic directions were obtained for 353 specimens from 160 sampling horizons (fig. 5A; Appendix 1): 96 specimens (27% of total specimens) from 46 sampling horizons from Kutz Canyon, 114 specimens (32% of total specimens) from 47 sampling horizons from Escavada Wash, 53 specimens (15% of total specimens) from 31 sampling horizons from Torreon West, and 90 specimens (25% of total specimens) from 36 sampling horizons from Torreon East.

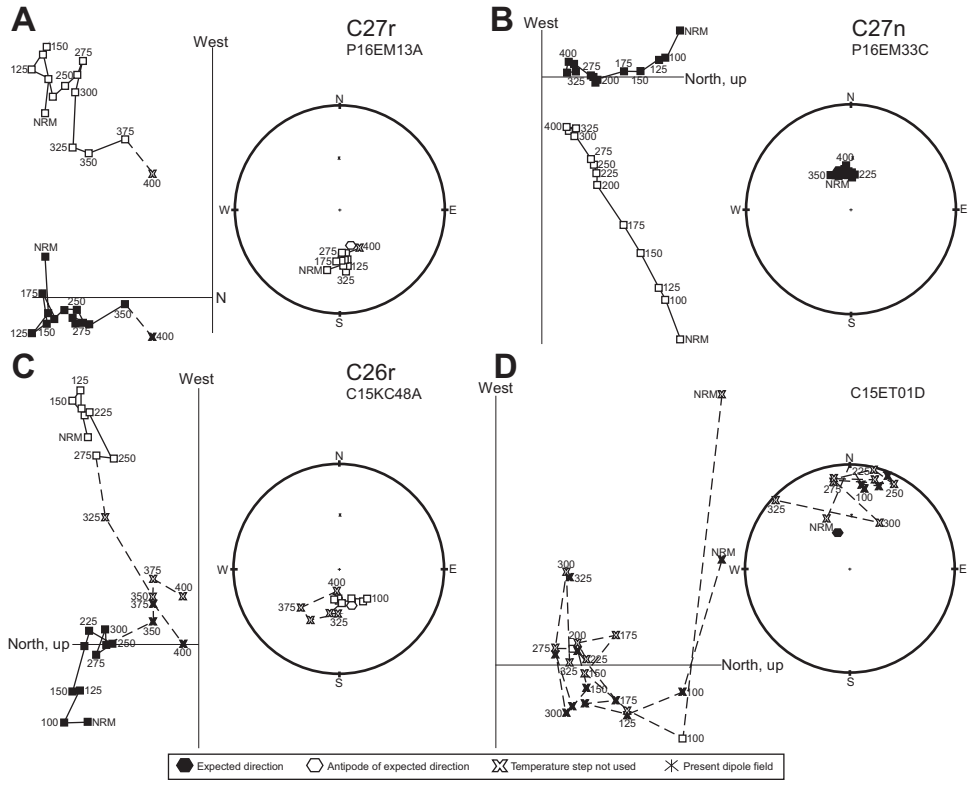

Fig. 4. Representative orthogonal end vector demagnetization diagrams and equal-area plots for each subset of data. (A) Demagnetization trajectory of a reversed polarity sample from C27r that allowed line-fitting to determine a characteristic direction (21% of data). (B) Demagnetization trajectory of a normal polarity sample from C27n where a line was calculated (27% of data). (C) Demagnetization trajectory of a reversed polarity sample from C26r where a line was calculated (17% of data). (D) Representative sample of erratic data that was not used for interpretations (35% of data).

Of these sampling horizons, sixty-six (41% of total sampling horizons) had at least three samples with statistically significant directions that could be used to calculate site-mean directions with α_{95}s <35°: 15 from Kutz Canyon, 26 from Escavada Wash, 8 from Torreon West, and 17 from Torreon East (fig. 5B; Appendix 2). The remaining 187 samples (35% of the data) had erratic demagnetization trajectories and coherent directions could not be obtained (fig. 4D).

The site-mean directions were averaged by section according to their polarity (fig. 5C), and also averaged at the formation-level, yielding normal (chron 27n) and reversed (chrons 26r and 27r) Upper Nacimiento Formation-mean directions (fig. 5D), and were used to calculate mean VGP latitude and longitude (table 2). The average Upper Nacimiento Formation direction for all the normal site-mean directions is oriented 352.8°, 56.1° (α_{95} = 4.9°, n= 28), whereas that of all the reversed polarity site-mean directions is oriented 164.4°, −55° (α_{95} = 5°, n = 38). The reversal test of McFadden and McElhinny (1990) returned a positive, class A test, indicating that these directions share a common mean at the 95 percent confidence level. These directions plot close to the expected Paleocene (62.5 Ma) direction of 341.8°, 60.1° recalculated from Torsvik and others (2008) and our mean sampling location. In addition, these directions also agree with the mean characteristic remanent direction

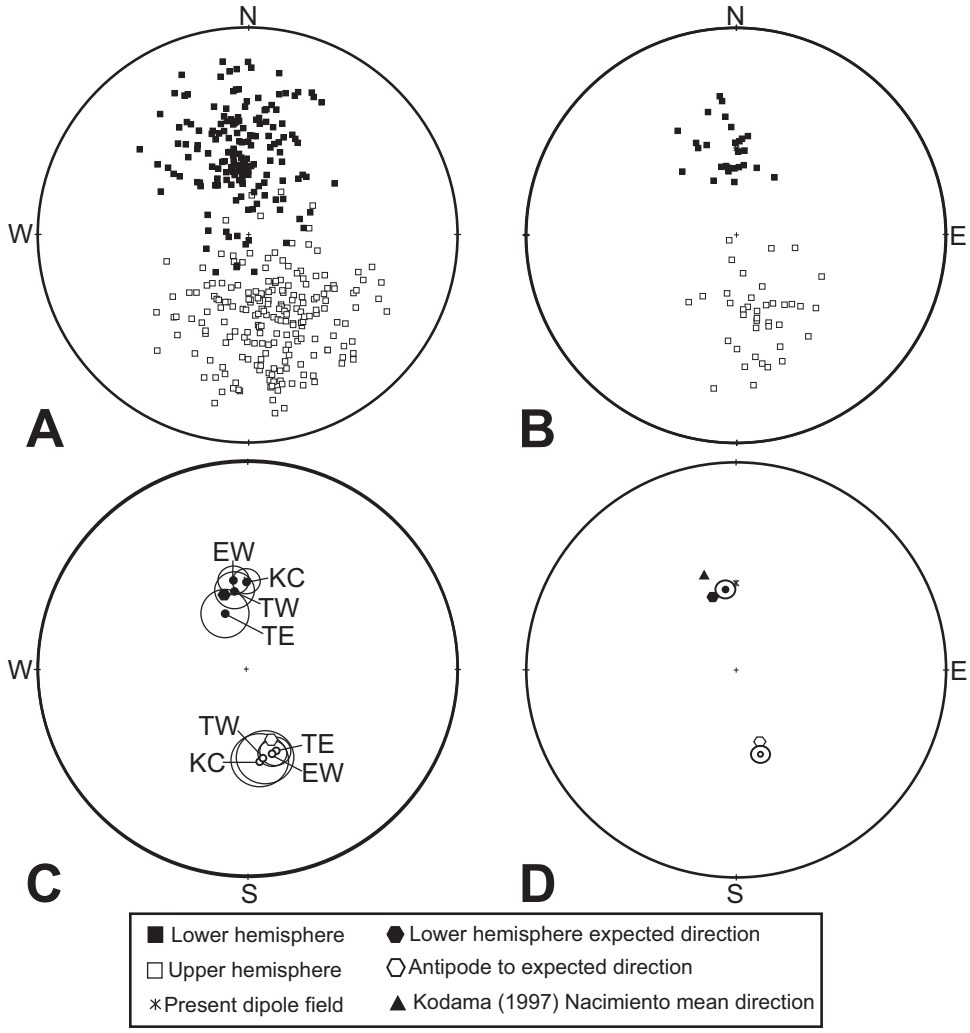

Fig. 5. (A) Equal-area plot of all characteristic magnetization directions obtained from this study. (B) Equal-area plot of normal and reversed site-mean directions from all sections. (C) Equal-area plot of normal and reversed site-mean directions averaged by section, and plotted alongside the present-day field position, the early Paleocene direction recalculated from Torsvik and others (2008) (see text for details), and the antipode to the early Paleocene direction. The ellipse around the mean direction represents the 95% confidence cone (Fisher, 1953). TW: Torreon West, TE: Torreon East, KC: Kutz Canyon, EW: Escavada Wash. (D) Upper Nacimiento Formation normal and reversed formation-mean directions plotted alongside the present-day field position, the early Paleocene direction recalculated from Torsvik and others (2008), the antipode to the early Paleocene direction, and the mean Nacimiento Formation direction reported by Kodama (1997). The ellipse around the mean direction represents the 95% confidence cone (Fisher, 1953).

of 342.1°, 49.6° (α_{95} = 7.1°, n = 20) for the Nacimiento Formation reported by Kodama (1997) after reversing all site-mean directions to normal polarity.

The mean VGP latitude and longitude calculated from all reversed (C26r and C27r) polarity sites is 77.2°N, 171.0°E (n = 38; A_{95} = 6.2), and that calculated from the normal polarity sites (C27n) is 84.1°N, 184.3°E (n = 28; A_{95} = 6.1), and can be compared to the expected paleopole of 74.9°N, 7.6°E recalculated from Torsvik and others (2008).

TABLE 2

Mean Paleomagnetic Directional Data From the Upper Nacaimiento Formation

Subset	*n*	D (°)	I (°)	k	a95 (°)	Pole (°N)	Pole (°E)	K	A95 (°)
Kutz Canyon normal sites	*9*	359.3	55.2	57.0	5.3	89.6	203.6	47.3	7.6
Kutz Canyon reversed sites	*6*	169.5	-53.7	12.3	19.9	79.5	174.8	9.3	23.1
Escavada Wash normal sites	*13*	349.7	54.6	20.1	9.5	81.9	174.4	12.2	12.4
Escavada Wash reversed sites	*13*	164.3	-55.3	30.4	7.6	77.6	168.3	18.6	9.9
Torreon West normal sites	*5*	351.2	58.8	116.3	7.1	82.1	195.1	83.0	8.4
Torreon West reversed sites	*3*	168.4	-54.2	38.1	20.3	81.5	162.0	28.6	23.5
Torreon East normal site	*1*	337.3	66.5	--	9.3	--	--	--	--
Torreon East reversed sites	*16*	161.6	-55.4	19.2	8.6	75.1	172.8	12.5	10.9
C27r- sites	*16*	166.7	-53.2	24.8	7.6	79.0	161.5	19.3	8.6
C27n - sites	*28*	352.8	56.1	32.5	4.9	84.1	184.3	20.8	6.1
C26r - sites	*22*	162.5	-56.3	20.4	7.0	75.6	178.5	12.6	9.1
C26r + C27r - sites	*38*	164.4	-55.0	22.3	5.0	77.2	171.0	14.9	6.2

Note: n – number of site-mean directions used to calculate the section and formation averages (see text for details); D – declination; I – inclination; k – Fisher's (1953) precision parameter; a95 – radius of 95% confidence cone around mean (Fisher, 1953); pole N and E – mean of virtual geomagnetic poles calculated from each line or site mean; K and A95 – Fisher statistics of paleomagnetic pole.

Figures 2 and 3 show the local polarity stratigraphy for each section including each specimen and site mean polarity and VGP latitude. At Kutz Canyon, the lower reversal is constrained within a 1 m interval while the upper reversal is constrained within a 4.5 m interval. Lower resolution on the latter is due to the presence of coarse grained sandstone at the top of the section that was not sampled (fig. 2; table 3). The presence of coarse grained sandstones and friable paleosols near the reversals at Escavada Wash resulted in poorer resolution. The lower reversal is constrained within an 8 m interval and the upper reversal is constrained within a 6.5 m interval (fig. 2; table 3). At Torreon West, the lower and upper reversals occur within 1.2 m and 0.4 m intervals, respectively (fig. 3; table 3). We assumed that the underlying deposits were reversed, based on the results of Taylor and Butler (1980). The lower and upper reversals at Torreon East are constrained within 0.5 m and 1 m intervals, and the underlying deposits were assumed to be reversed (fig. 3; table 3).

Rock Magnetism

Rock magnetic analyses show that the upper Nacimiento Formation has a mixed magnetic mineralogy. Low temperature magnetometry for a representative sample of a black slickensided paleosol shows a two-fold increase on cooling of the RTSIRM and the magnetite Verwey transition (~120 K), indicating that goethite and magnetite coexist in the same specimen (for example, figs. 6A and 6B).

High temperature susceptibility curves for representative red calcareous paleosol specimens decreased until ~125 °C and subsequently dropped at ~550 °C, suggesting the presence of goethite and titanomagnetite (figs. 6C and 6I). Low temperature magnetic measurements for these specimens also reveal a hematite Morin transition (~260 K) and a diffuse Verwey transition between ~130 to 90 K, indicating the presence of magnetite in different oxidation states (maghemite).

Low temperature magnetometry measurements from a brown, weakly-developed paleosol specimen reveal a magnetite Verwey transition and a ~two-fold increase of

TABLE 3

Stratigraphic Position of Polarity Zone Boundary

Local polarity zone	Chron	Location	Lowermost sample in chron	Uppermost sample in chron	Stratigraphic position of base (m)	Stratigraphic position of top (m)	Chron thickness (m)	Uncertainty (m)
A-	C27r	Kutz Canyon	KC45A	KC13A	0.0	29.0	29.0	± 0.5
		Escavada Wash	EM01A	EM20C	0.0	38.0	38.0	± 4.0
		Torreon West	TW01A	TW14A	0.0	36.7	36.7	± 0.6
		Torreon East	ET02A	ET11D	0.0	31.8	31.8	± 0.25
B+	C27n	Kutz Canyon	KC15A	KC39D	29.0	64.5	35.5	± 2.75
		Escavada Wash	EM21A	EM42C	38.0	72.3	34.3	± 7.25
		Torreon West	TW15B	TW23D	36.7	72.2	35.5	± 0.8
		Torreon East	ET12A	ET40C	31.8	57.5	26.0	± 0.75
C-	C26r	Kutz Canyon	KC41A	KC44D	64.5	69.0	4.5	± 2.25
		Escavada Wash	EM45B	EM50C	72.3	77.6	5.3	± 3.25
		Torreon West	TW24A	TW38C	72.2	78.4	6.2	± 0.2
		Torreon East	ET18C	ET35C	57.5	74.0	16.5	± 0.5

Note: Uncertainty is the number of meters between samples of opposing polarity.

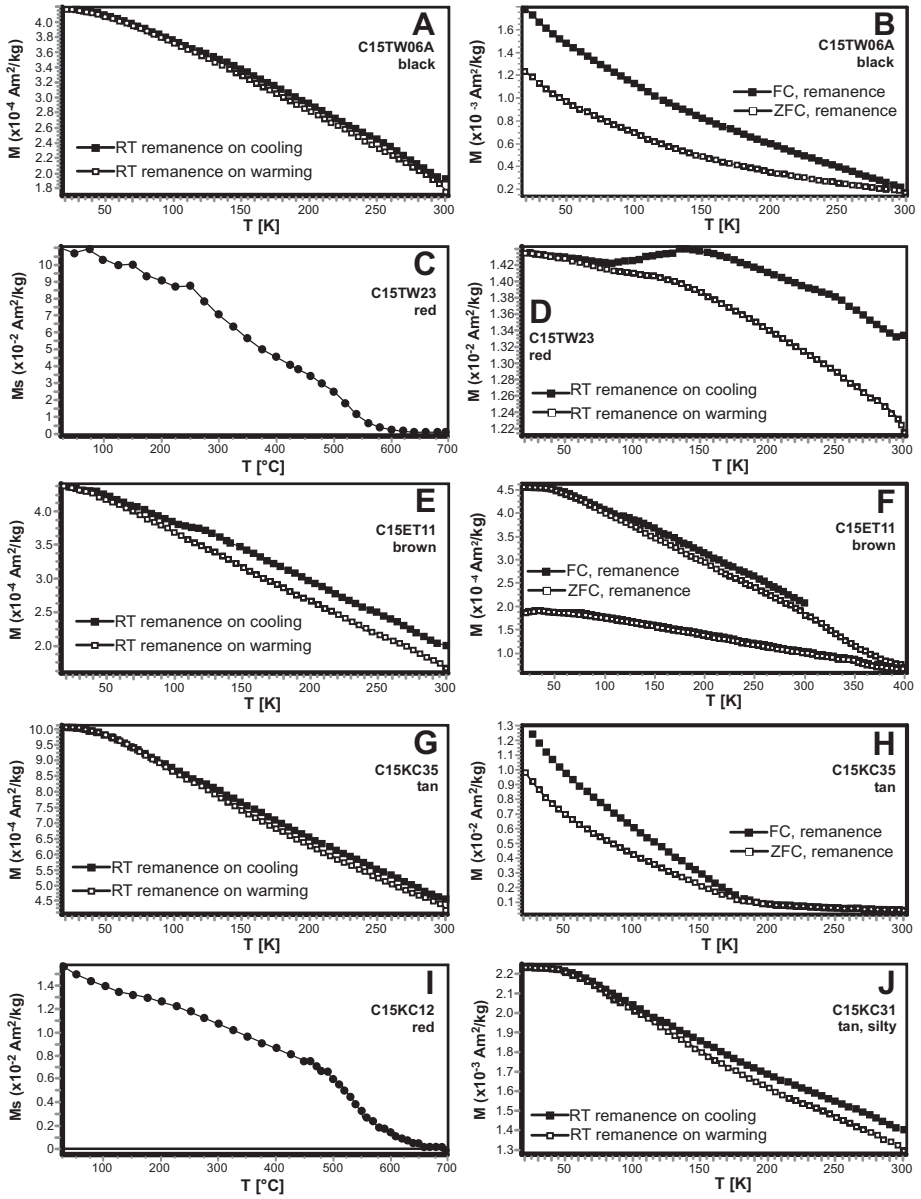

Fig. 6. Rock magnetic analysis results including low temperature magnetization curve of representative samples and high temperature VSM (vibrating sample magnetometer) curves of saturation magnetization. Room temperature (RT) plots show magnetization measurements upon cooling and warming between 20K and room temperature (300K) following the application of saturation isothermal remanent magnetization (SIRM) at room temperature. FC (field-cooled) and ZFC (zero field-cooled) plots show magnetization during warming following a sustained direct current field of 2.5 T during cooling (FC), and magnetization during warming following a SIRM imparted at low temperature (ZFC). (A) RT curves for a black, slickensided paleosol sample indicating goethite and magnetite. (B) FC/ZFC curves for a black, slickensided paleosol sample indicating goethite. (C) High temperature VSM curve for a red, calcareous paleosol sample indicating goethite, titanomagnetite, and hematite. (D) RT curves for a red, calcareous paleosol sample indicating maghemite. (E) RT curves for a brown paleosol sample indicating magnetite and goethite. (F) FC/ZFC curves from the goethite test for a brown paleosol sample indicating goethite and titanohematite. (G) RT curves for a tan paleosol sample indicating magnetite and goethite. (H) FC/ZFC curves for a tan paleosol sample indicating Al-substituted goethite. (I) High temperature VSM curves for a red, calcareous paleosol indicating goethite, titanomagnetite, magnetite, and hematite. (J) RT curves for a tan, silty weakly-developed paleosol sample indicating titanomagnetite and magnetite (see text for details).

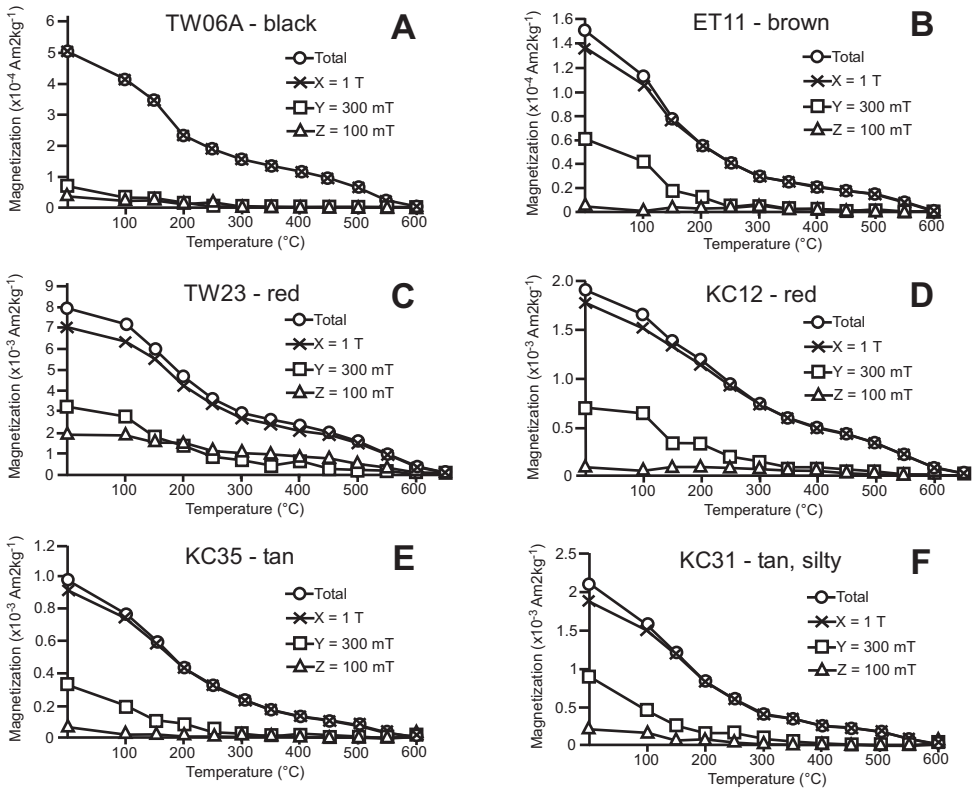

Fig. 7. Thermal demagnetization of orthogonal isothermal remanent magnetization (IRM) imparted along X, Y, and Z axes for six specimens following Lowrie (1990) indicating a mixed magnetic mineralogy with goethite as the dominant carrier.

magnetic remanence upon cooling, indicating the presence of goethite (fig. 6E). A goethite test performed on the same specimen (fig. 6F) shows that remanence is lost when warming to 400 K as goethite is demagnetized through its Néel ordering temperature. However, some magnetic remanence persists upon subsequent cooling to 20 K indicating the presence of a high coercivity phase that is not demagnetized at low temperature, nor up to 400 K, likely indicating the presence of titanohematite.

RTSIRM curves for a representative specimen of a tan paleosol suggests both magnetite and goethite from the presence of the Verwey transition and an increase of remanence upon cooling (fig. 6G). FC-ZFC-LTSIRM curves converge at 190 K, which indicates Al-substituted or nano-goethite (fig. 6H). RTSIRM curves for a tan, silty weakly-paleosol sample have a separation at 90 K indicating maghemite and a slight Morin transition indicating hematite (fig. 6J).

Triaxial-IRM Lowrie tests were performed to determine the relative abundance of magnetic carriers in each sample. For all samples analyzed the majority of the IRM is held by grains whose coercivities are greater than 1 T (fig. 7). The largest remanence drop occurs between 100 to 150 °C suggesting goethite is the most abundant mineralogy in the samples. Some samples also show a decrease in remanence between 150 to 200 °C suggesting titanohematite may also be present. Remanence remaining after 200 °C is likely held by pigmentary hematite for samples TW23 and KC12, supported by

the loss of remanence between 600 to 650 °C, red coloring, and the low temperature rock magnetometry experiments. In all other samples, the remaining remanence is likely maghemite that inverted to hematite upon heating above ~450 °C. All samples, except TW06A, also show remanence held by the 300 mT curve up to ~300 °C, indicating the presence of magnetite/maghemite.

Detrital Sanidine Dating

The age probability plot for sample HJ16-SJ-11 from Escavada Wash is shown in figure 8. The sample is dominated by Paleocene grains where 66 of the 86 crystals give a weighted mean age of 62.48±0.02 Ma. Older grains concentrate around 68 and 70 Ma with 8 crystals giving apparent ages >200 Ma. The dominance of a high proportion of grains near 62.5 Ma suggests that this sample may be a minimally reworked tephra layer such that the maximum deposition age closely approximates the actual deposition age.

DISCUSSION

Magnetic Mineralogy

The upper Nacimiento Formation has a mixed magnetic mineralogy with titanohematite and maghemite as the characteristic remanent magnetization carriers. Goethite is also present in all lithologies and dominates the low-temperature magnetic measurements, however it does not contribute to the characteristic remanence direction. Titanohematite is likely present in most samples, supported by the drop in remanence between 150 to 200 °C in the orthogonal IRM measurements and low temperature magnetometry measurements. Figure 6F shows that during the goethite test, there is an increase in remanence from room temperature to low temperatures after the goethite is removed. The phase must be high coercivity because it persists after the goethite test and the 1T orthogonal demagnetizations (fig. 7) and must have an ordering temperature above 400 K since it survives heating to that point (fig. 6F). These characteristics collectively indicate titanohematite as a characteristic remanent magnetization carrier, in agreement with the observations of Butler and Lindsay (1985). However, although titanohematite along with maghemite constitute the primary magnetic mineralogy, titanohematite does not appear to be the most abundant remanence carrier as suggested by Butler and Lindsay (1985). It is possible that given the broad sample spacing in Butler and Lindsay (1985), our samples do not overlap. Nonetheless, the presence of detrital titanohematite in the sections does support their conclusion that sediments were derived from the volcanic San Juan Mountains to the north. Goethite is the most abundant magnetic mineral and likely an alteration product, whereas the titanohematite is likely detrital. Agreement of the characteristic remanent directions obtained in this study to those reported by Kodama (1997) for the Nacimiento Formation confirm the primary nature of the magnetizations residing in maghemite and titanohematite. Kodama (1997) performed an inclination-correction study of the formation, and reported a 7 to 8° inclination bias, however, it should be noted that any inclination shallowing would not affect a reversal stratigraphy.

Relationship of Polarity Stratigraphy to GPTS

Taylor and Butler (1980) reconstructed the magnetic polarity stratigraphy at Torreon West, Torreon East, and Kutz Canyon and correlated the strata to C26r-C25r based on previous work by Lindsay and others (1978) and Taylor (ms, 1977). Butler and Lindsay (1985) revised the correlation of the polarity zones to the GPTS to correlate the late To2-To3 deposits at Torreon Wash and Kutz Canyon with C27r through C26r. We use the Butler and Lindsay (1985) interpretations for the base of the Nacimiento Formation and correlate the A−, B+, and C− magnetozones from the

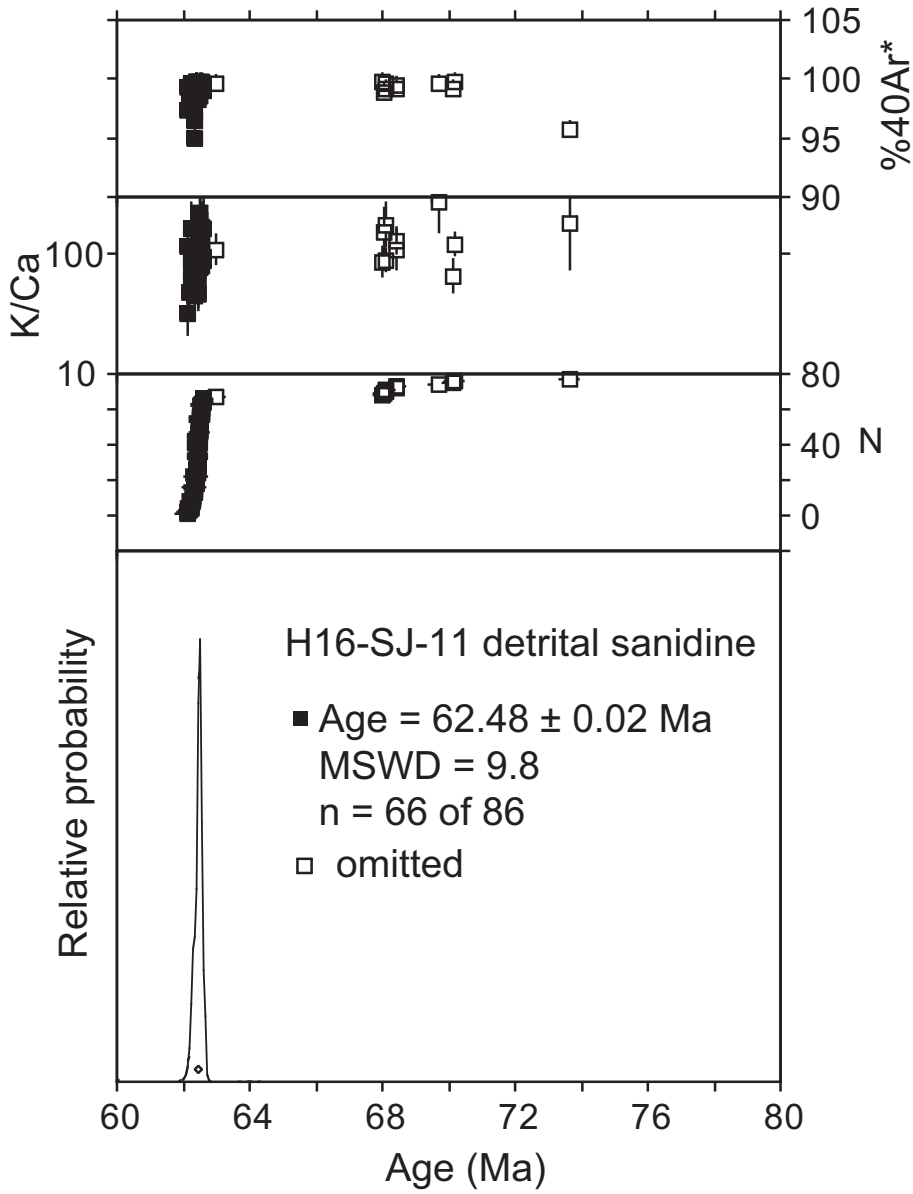

Fig. 8. Age probability diagram for the analyzed sample, H16-SJ-11. The plot shows, from bottom to top, the age probability distribution spectrum for the data shown with solid squares, distribution of individual single-crystal ages with 1σ errors, K:Ca ratios, and percentage of radiogenic 40Ar*.

sections in our study to C27r-C26r (figs. 2 and 3). The polarity stratigraphy of the To2-To3 strata of Escavada Wash has not been previously published. This section also contains A−, B+, and C− magnetozones. A detrital sanidine age of 62.48±0.02 Ma from 64 meters in the section, within the B+ magnetozone, indicates correlation to C27n (Ogg, 2012). Thus we can correlate the underlying A− interval to C27r and the overlying C+ interval to C26r.

Sediment Accumulation Rates and Section Durations

Given that the entire C27n polarity zone (local polarity B+) occurs in each section and the temporal duration of the corresponding polarity chron has been estimated (Ogg, 2012), we were able to calculate mean sediment accumulation rates for each section shown in table 4. Uncertainty associated with the duration of C27n (Ogg, 2012) was taken from Cande and Kent (1992), where the uncertainty in the time scale was assumed to be the same as the uncertainty in the width of the magnetic anomaly for C27n, which was ±6.9 percent. Uncertainties for the calculated sediment accumulation rates are asymmetrical because different stratal thicknesses and durations for C27n were used. The maximum sediment accumulation rate was calculated by dividing the maximum thickness of C27n strata by the minimum duration of C27n. The minimum sediment accumulation rate was calculated by dividing the minimum thickness of C27n strata by the maximum duration of C27n. Kutz Canyon, Torreon West, and Escavada Wash have similar mean sediment accumulation rates ranging from 115.7 to 119.9 m/myr and the rates are indistinguishable when factoring in their uncertainties. Torreon East has a lower sediment accumulation rate of 87.0 m/myr (−8.0, +9.0 m/myr). Large channel bodies within the C27n interval of this section suggest that erosion into the landscape occurred, reducing the overall preserved sediment thickness and resulting in a lower calculated accumulation rate. As a result, application of the calculated mean sediment accumulation rate to the remainder of the section may overestimate the amount of time the section spans if less erosion or more sediment accumulation occurred over the C27r and C26r intervals. The similarity of sediment accumulation rates at Kutz Canyon, Escavada Wash, and Torreon West suggests that sedimentation was similar across the basin as sampled sections are located both near the basin center (Kutz Canyon) and southern edges (Torreon West and Escavada Wash). This similarity is important because the Nacimiento Formation thins from north to south in the basin. The work of Taylor (ms, 1977) indicates that the entire C27r through C27n section is nearly twice as thick in Kutz Canyon (150 m) as in Torreon West (58 m). Consequently, sediment accumulation rates at Kutz Canyon for the lower part of the Nacimiento Formation (that is, early in C27r) must have been much greater than in Torreon Wash, but equalize higher in the section (Taylor, ms, 1977). This interpretation is supported by sediment accumulation rates calculated for C27r in Kutz Canyon based on the magnetostratigraphy of Taylor (ms, 1977), which suggest mean rates of ~120 to 150 m/myr compared to preliminary mean accumulation rates for C27r-C28n from Kutz Canyon of ~180 m/myr (Peppe, unpublished data).

The duration of each section and the ages of all of the mammal fossil localities within each section was determined by extrapolating each section's C27n calculated sediment accumulation rate to the top and the bottom of each section (fig. 9; tables 1 and 4). Uncertainties for the duration of each section are also asymmetrical because the maximum and minimum sediment accumulation rates were used to calculate the uncertainties. Kutz Canyon is estimated to span the least amount of time, 580 kyr (−90, +100 kyr), from 62.76 to 62.18 Ma. Escavada Wash spans 750 kyr (−190, +280 kyr) from 62.85 to 62.10 Ma. Torreon West spans 650 kyr (−80, +80 kyr) from 62.82 to 62.17 Ma. Torreon East is calculated to span 870 kyr (−100, +100 kyr) from 62.88 to 62.01 Ma, but as noted above, the presence of large channel bodies within the C27n interval suggests that erosion occurred and the calculated sediment accumulation rate may be an underestimation for the remainder of the section, which results in an overestimate of the duration of deposition in the Torreon East section.

TABLE 4

Calculated Sediment Accumulation Rates and Durations of Polarity Zones

	Kutz Canyon	Escavada Wash	Torreon West	Torreon East
C27n duration* (myr)	0.296 ± 0.02	0.296 ± 0.02	0.296 ± 0.02	0.296 ± 0.02
Calculated sediment accumulation rate (m/myr)	119.9 (-16.3, +18.7)	115.7 (-30.3, +34.7)	119.9 (-10.1, +11.6)	87.0 (-8.0, +9.0)
Calculated duration of C27r strata (myr)	0.24 (-0.03, +0.04)	0.33 (-0.10, +0.16)	0.30 (-0.03, +0.04)	0.36 (-0.04, +0.04)
Calculated duration of C26r strata (myr)	0.04 (-0.02, +0.02)	0.12 (-0.05, +0.08)	0.05 (-0.01, +0.01)	0.21 (-0.02, +0.03)
Calculated age of section base (Ma)	62.76 (-0.05, +0.06)	62.85 (-0.12, +0.18)	62.82 (-0.05, +0.06)	62.88 (-0.06, +0.06)
Calculated age of section top (Ma)	62.18 (-0.04, +0.04)	62.10 (-0.10, +0.07)	62.17 (-0.03, +0.02)	62.01 (-0.05, +0.04)
Calculated total section duration (myr)	0.58 (-0.09, +0.10)	0.75 (-0.19, +0.28)	0.65 (-0.08, +0.08)	0.87 (-.10, +.10)

* C27n duration from Ogg (2012), uncertainty was taken from Cande and Kent (1992), where the uncertainty in the time scale was assumed to be the same as uncertainty in the width of the magnetic anomaly for C27n, which was ± 6.9%. Uncertainties associated with the sediment accumulation rates, strata durations, section ages, and section durations are shown in parentheses. Sediment accumulation uncertainties are asymmetrical because different stratal thicknesses and durations for C27n were used. The maximum sediment accumulation rate was calculated by dividing the maximum thickness of C27n strata by the minimum duration of C27n. The minimum sediment accumulation rate was calculated by dividing the minimum thickness of C27n strata by the maximum duration of C27n. The maximum and minimum sediment accumulation rates were used to calculate uncertainties for durations and ages, also resulting in asymmetrical uncertainties.

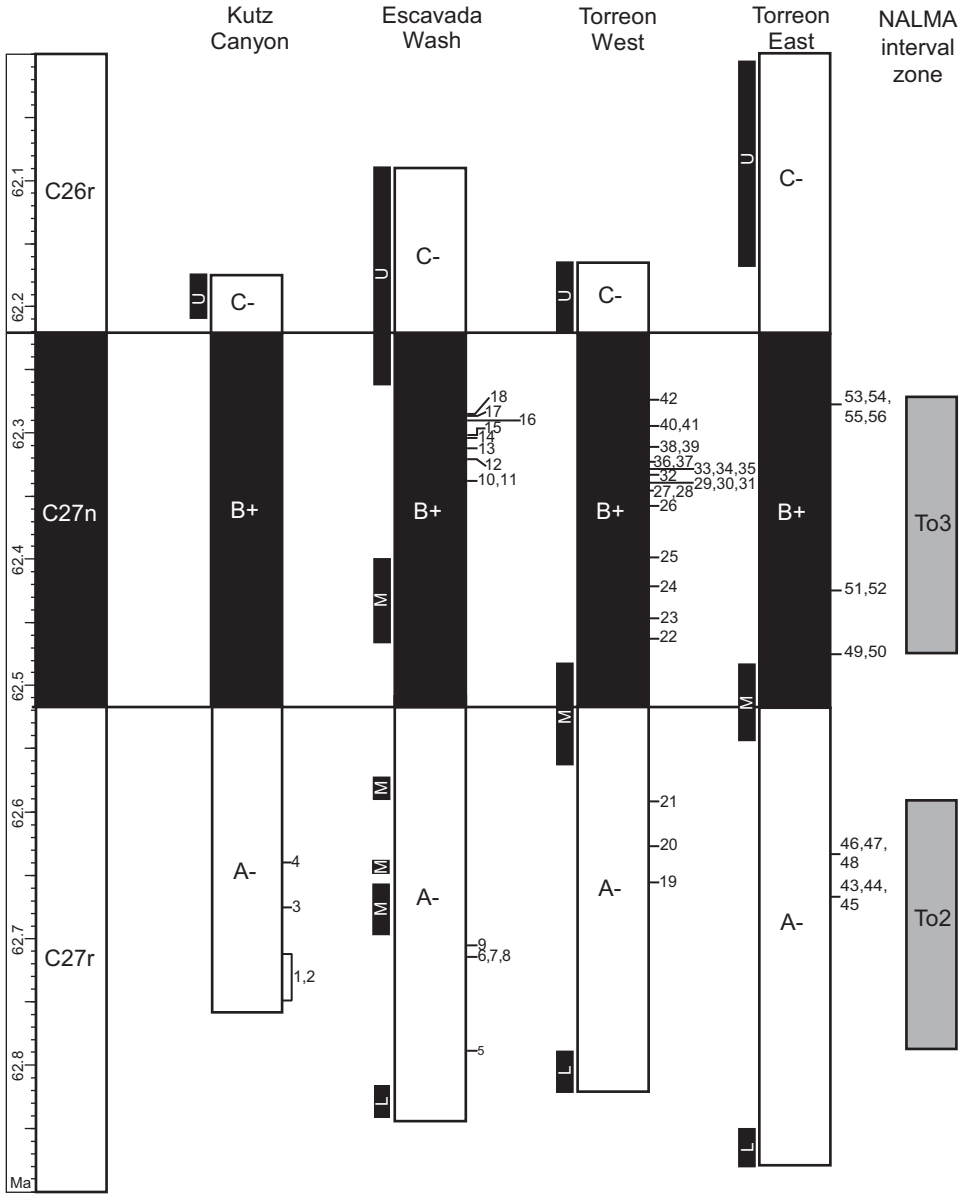

Fig. 9. Chronostratigraphy of the Upper Nacimiento Formation showing the age and calculated duration of the Kutz Canyon, Escavada Wash, Torreon West, and Torreon East sections. Time scale from Ogg (2012) is shown to the left. Lithologies are highlighted for each section along with fossil localities. Fossil localities 1–4 from Kutz Canyon, 5–18 from Escavada Wash, 19–42 from Torreon West, and 43–56 from Torreon East are described in table 1.

Evolution of the San Juan Basin

The calculated sediment accumulation rates for C27n, which are considerably lower than those for C27r, suggest that the basin was probably mostly filled prior to the end of C27r (late To2) and sedimentation equalized across the basin during the end of C27r through the start of C26r. These findings support the three phase subsidence

model proposed by Cather (2004) that determined a phase of subsidence from ~74 to 67 Ma resulted in the deposition of the Nacimiento Formation. Following this phase of subsidence, the space available for sediments to fill likely decreased with time throughout the early Paleocene so that during the late part of C27r through early in C26r (~63–62 Ma) there was little accommodation space in the basin. This lack of accommodation space likely caused the unconformity between the upper Nacimiento Formation and the overlying Eocene San Jose Formation. Sedimentation resumed in the Eocene once additional accommodation space was created, the third phase of subsidence documented by Cather (2004).

This interpretation of equalized accommodation space in the San Juan Basin plausibly explains the dominance of sheet sands rather than channels throughout the top of C27r-C26r interval in all four sections (figs. 2 and 3) and the similar sediment accumulation rates from basin center to basin margin (table 3). If accommodation was low in the basin during this time, the sediment transport capacity of a channel was likely frequently exceeded, resulting in unconfined flow and deposition of laterally continuous sheet sands. This evidence for unconfined flow also suggests that the Nacimiento Formation records the progradation and/or aggradation of a distributive fluvial system (DFS), characterized by a radial channel pattern and aggradational deposition below the point where flow becomes unconfined (Weissmann and others, 2010; Hobbs, ms, 2016). Low accommodation and fan progradation could also explain the presence of better drained soils embodied by red, calcareous paleosols. Well-developed soils are expected during accommodation minimums and fan progradation because the distance to the water table increases and distance to the source decreases (Weissmann and others, 2010; Atchley and others, 2013). However, it is important to note that variations in climate may have also been an important contributing factor in generating these features.

Mammalian Biostratigraphy

The Nacimiento Formation contains the only deposits in North America where mammalian turnover between To2-To3 can be constrained, and temporal constraint of this turnover may provide a better understanding of possible driving mechanisms. Using estimated sediment accumulation rates (table 4), an age was assigned to each To2 and To3 mammal locality in each section (table 1, fig. 9). Our magnetostratigraphy for the upper Nacimiento Formation corroborates the interpretation of Lofgren and others (2004) that the To2 NALMA interval zone occurs within C27r and the To3 NALMA interval zone occurs within C27n. Additionally, there is no evidence that the turnover is diachronous across the San Juan Basin.

Both late To2 and To3 mammals are found at Escavada Wash, Torreon West, and Torreon East, and thus these areas are the best locations to determine the timing of the To2-To3 turnover. At Escavada Wash the youngest To2 locality (L-10350) occurs at 62.71 Ma (−0.07, +0.08 myr) and the oldest To3 localities (L-09981 and L-10444) occur at 62.35 Ma (−0.10, +0.05 myr), which indicates the turnover occurred over 360 kyr (−120, +180 kyr). At Torreon West, the youngest To2 locality (L-08180) occurs at 62.59 Ma (−0.02, +0.03 myr) and the oldest To3 locality (L-09173) occurs at 62.46 Ma (−0.02, +0.03 myr) for a duration of 130 kyr (−50, +50 kyr) between NALMA interval zones. At Torreon East the youngest To2 localities (L-07583, L-04954, and L-04950) occur at 62.63 Ma (−0.02, +0.04 myr) and the oldest To3 localities (L-10013 and L-10432) occur at 62.47 Ma (−0.02, +0.04 myr) for a duration of 160 kyr (−60, +60 kyr) between the interval zones. When using the youngest To2 locality in the basin, which is a locality in Torreon West (L-08180), and the oldest To3 localities, which are localities in Torreon East (L-10013 and L-10432), the duration between the To2-To3 NALMA interval zones is 120 kyr (−60, +50 kyr) and occurred between 62.59 to 62.47 Ma. This indicates that To2-To3 turnover occurred over a relatively short period of

time and suggests that the To2-To3 transition was probably not driven exclusively by typical patterns of origination and extinction. Instead, they may be due to very rapid rates of speciation, migration of new taxa into the basin, or both. The driver of an increase in mammalian speciation rates and/or dispersal of taxa into the basin is uncertain, but we posit that it was driven by external factors such as environmental change associated with changes in basin dynamics or regional/global changes in climate. Further work focused on reconstructing the environment and climate of this interval will help resolve this question.

CONCLUSIONS

The polarity zones for the four sections in this study, Kutz Canyon, Escavada Wash, Torreon West, and Torreon East, are correlated to chrons C27r-C26r of the geomagnetic polarity time scale. This study is the first published polarity stratigraphy for the Escavada Wash section, and a $^{40}Ar/^{39}Ar$ detrital sanidine age further constrains the age of the section. Rock magnetic analyses indicate that although goethite is the most abundant magnetic mineral, titanohematite and maghemite carry the characteristic remanent magnetization. The age model for the upper Nacimiento Formation presented here has important implications for the evolution of the San Juan Basin and the timing and nature of the To2-To3 mammalian turnover. Our results indicate that sediment accumulation rates near the basin center were similar to those near the basin edge, which signals that from the end of C27r through the start of C26r sediment accumulation rates had equalized across the basin. This suggests that the deposition of the upper Ojo Encino Member occurred during a basin accommodation minimum, which was associated with the progradation of a distributive fluvial system across the basin. The later unconformity between the Paleocene Nacimiento Formation and the lower Eocene San Jose Formation was likely driven by a lack of accommodation in the San Juan Basin and sedimentation could not resume until additional accommodation space was created in the Eocene. This is consistent with Cather's (2004) three phase model of basin subsidence.

Estimates of sediment accumulation rates for strata in the Escavada, Torreon West and East, and Kutz Canyon sections were used to determine the age to each To2-To3 fossil locality in those sections, and in turn constrain the duration of the To2-To3 turnover. These results indicate that the To2-To3 turnover was rapid and occurred over ~120 kyr (−60, +50 kyr) between 62.59 and 62.47 Ma. The rapid nature of the mammalian turnover suggests that there was likely an external forcing factor, such as an environmental change driven by the progradation of the distributive fluvial system across the basin and/or changes in regional or global climate.

ACKNOWLEDGMENTS

This work was supported by SEPM (CL), National Science Foundation EAR-132552 (DP), −1325612 (RS), −0207750 and −1325544 (TEW), American Chemical Society Petroleum Research Fund (PRF#52822-DN18) (DP), Baylor University Department of Geosciences' Dixon Fund (CL, TL), and the University of Minnesota Institute for Rock Magnetism visiting student fellowship (CL). This is IRM publication #1706. We thank K. Kodama, D. Lofgren, and one anonymous reviewer for their helpful comments and P. Gingerich for the editorial assistance. Thanks to A. Flynn, A. Davis, J. Milligan, and A. Baumgartner for assistance with sample collection and section measuring.

APPENDIX 1

Paleomagnetic data: lines

Location	Paleosol #	Strat level (m)	Sample	Temp. steps	Strat. Declination	Strat. Inclination	MAD	Strat. VGP latitude	Strat. VGP longitude
Kutz	P34	1	C15KC45A	200,250,275	174.3	-39.3	19.1	-74.9	272
Kutz	P34	1	C15KC45B	250-300	197.2	-68.1	18.1	-70.9	106.5
Kutz	P34	1	C15KC45C	250-300	163.8	-26	4	-63	288.7
Kutz	P35	2	C15KC46C	250-300	136.3	-29.2	11.7	-46	325.5
Kutz	P35	2	C15KC46D	200-250	146	-33.8	8.3	-55.2	320.3
Kutz	P36	2	C15KC47A	225,250,300	127.6	-73.2	16.6	-49.7	32.8
Kutz	P37	4.5	C15KC48A	250-300	178	-64.2	9.9	-80.4	63.7
Kutz	P37	4.5	C15KC48B	250-300	157.4	-69.8	8.3	-66.8	36.8
Kutz	P37	4.5	C15KC48C	150,225,250	125.3	-65	12.6	-48.7	14.5
Kutz	P1	15.5	C15KC01B	225-275	171.9	-41.5	9.3	-75.6	283.2
Kutz	P1	15.5	C15KC01D	250-300	189.4	-24.1	18.8	-64.7	230.2
Kutz	P1	16	C15KC02A	175, 250, 275	251.3	-56.2	20	-34.2	138.7
Kutz	P1B	16	C15KC02B	150-225	173.1	-58.2	5.4	-84	7.8
Kutz	P1	16	C15KC02D	250-275	129.6	-62.3	5.8	-51.4	8.7
Kutz	P2	18.5	C15KC03A	150-200	217.7	-29.9	9.8	-50.9	183.5
Kutz	P3	19	C15KC04A	175, 200, 250	65.9	-62.5	8.3	-10.1	30.1
Kutz	P3	19.5	C15KC05A	150-200	167.8	-28.6	7.6	-66.1	282.4
Kutz	P4	20.5	C15KC06A	150-200	138.9	-24.8	3.1	-46.4	320.3
Kutz	P5	21.8	C15KC07B	150-200	145.9	-50.5	12.4	-61.4	341.6
Kutz	P5	21.8	C15KC07C	250-300	171.7	-32.9	4.9	-70.0	275.8
Kutz	P5	21.8	C15KC07D	125-175	160.3	-23.6	16.7	-060.0	293.3
Kutz	P6	24.8	C15KC08C	175-225	221.2	-59.4	9.3	-57.8	142.7
Kutz	P7	26.3	C15KC09A	250-300	116.7	-31.1	19.3	-31.2	340.5
Kutz	P7	26.3	C15KC09C	275-325	197	-28.5	14.9	-63.9	212.3
Kutz	P7	26.5	C15KC10A	250-300	183.7	-25.9	11.1	-66.9	242.9
Kutz	P7	26.5	C15KC10B	250-300	191.1	-18.1	11	-61	229
Kutz	P7	26.5	C15KC10D	250-300	190.9	-35	19.1	-70.3	220.1
Kutz	P8	27.8	C15KC11B	225-300	171.6	-13.9	12.3	-59.6	268.7
Kutz	P8	27.8	C15KC11D	150-200	220.7	-46.4	7.7	-54.7	164.6
Kutz	P9	27.5	C15KC12A	250-300	176.7	-46.2	4	-80.6	270.3
Kutz	P9	27.5	C15KC12C	250-300	182.7	-40.4	10.1	-76.4	241.5
Kutz	P9	27.5	C15KC12D	250-300	186.5	-46.9	9.2	-79.3	245.8
Kutz	P10	28.5	C15KC13A	250-300	141.9	-55.2	14.7	-59.4	352.2
Kutz	P11	29.5	C15KC15A	250-300	103.4	74.8	13.4	25.7	283.1
Kutz	P11	29.5	C15KC15B	NRM, 125, 150	331.7	38.5	4.1	61.3	138.8
Kutz	P11	29.5	C15KC15D	NRM, 125, 150	355.3	44.4	7.5	78.8	94.5
Kutz	P11	30.5	C15KC16A	NRM, 125, 150	22.4	73.4	7.3	63.1	277.6
Kutz	P11	30.5	C15KC16B	NRM, 125, 150	350.6	62.3	3.7	79.9	209.7
Kutz	P11	30.5	C15KC16C	125, 225, 275	340.2	47.4	5.3	71.6	142.2
Kutz	P12s	31.5	C15KC17A	150-200	334.7	44.1	15.2	66	143
Kutz	P12	31.5	C15KC17B	250-300	351.6	17	15.8	61.2	89.5
Kutz	P12	31.5	C15KC17D	125-175	355.5	53.2	2.8	85.4	126.7
Kutz	P13	32.5	C15KC18A	250-300	16.9	65.7	3.7	73.1	294.3
Kutz	P13	32.5	C15KC	150-200	2.4	63.2	5.1	81.6	263.8
Kutz	P13	32.5	C15KC18D	225-275	349	58.2	4.5	81	180.7
Kutz	P13	32.8	C15KC19A	250-300	357.1	47.6	2.9	81.8	90.3
Kutz	P13	32.8	C15KC19B	225-275	352.4	45.6	13.8	78.6	108.5
Kutz	P13	32.8	C15KC19C	200-250	24.6	58.3	6.2	70.4	327.3
Kutz	P14	33.5	C15KC20B	175,225,275	1.5	54.7	5.2	88.2	27.9
Kutz	P14	33.5	C15KC20C	125,175,200	347.8	56.7	4.1	80.2	170.3
Kutz	P14	33.5	C15KC20D	125,150,200	5.7	45.6	8.2	79.4	43.4
Kutz	P14	33.8	C15KC21A	200, 275, 325	274.7	74.5	9	33.5	216.7
Kutz	P14	33.8	C15KC21B	150-200	337.6	18.1	20	56	114.4
Kutz	P14	33.8	C15KC21C	NRM, 125, 200	23.6	47	9.7	68.5	358
Kutz	P15	35.5	C15KC22A	125,175,200	2.2	50.7	4.7	84.6	51.7
Kutz	P15	35.5	C15KC22D	NRM, 125, 150	264.5	82.3	15.6	33.6	233.9
Kutz	P16	36.2	C15KC23A	225,250,300	354	31.3	14.3	69.7	88.9
Kutz	P16	36.2	C15KC23D	125-175	14.6	30.3	8.9	66	35.6
Kutz	P16	36.5	C15KC24A	225,250,300	14	54.5	4.4	78.6	345.3
Kutz	P16	36.5	C15KC24C	225-275	354.6	44.5	6.7	78.7	97.6
Kutz	P16	36.5	C15KC24D	225,275,300	11.3	49.9	4.8	49	10.5
Kutz	P17	39.7	C15KC25C	125, 175, 225	4.2	34.4	13.8	72	59.1
Kutz	P18	39.3	C15KC26C	NRM, 125, 175	10.1	36.9	11.4	71.8	40.4
Kutz	P19	39.8	C15KC27D	125-175	341.7	69.4	5.3	69.1	220.2
Kutz	P20	41.5	C15KC28A	125-175	349.3	43.8	11.7	75.8	115.1
Kutz	P20	41.5	C15KC28C	250-300	332.9	40.1	16.5	62.9	139.3
Kutz	P21	43	C15KC29B	125, 200, 225	25.2	27.7	7.3	58.7	19.6
Kutz	P21	43	C15KC29C	125, 175, 325	332.2	59.6	15.2	68	180.9
Kutz	P22	44	C15KC30C	NRM, 125, 250	73.2	69.2	8.8	37.9	299.3
Kutz	P22	44	C15KC30D	NRM, 125, 150	10.8	21.9	13	63	48.2
Kutz	P23	44.6	C15KC31C	125-175	359.4	36.1	13.4	73.5	74.1
Kutz	P24B	46	C15KC32B	125, 200, 225	16	77.7	14.3	58.7	264.3
Kutz	P24	46	C15KC32C	250-300	346	63	12	76.7	203.3
Kutz	P24	46	C15KC32D	125, 175, 200	359.6	65.1	4.8	79.4	250.6

APPENDIX 1
(continued)

Location	Paleosol #	Strat level (m)	Sample	Temp. steps	Strat. Declination	Strat. Inclination	MAD	Strat. VGP latitude	Strat. VGP longitude
Kutz	P25	47	C15KC33D	100-150	70.3	64.5	9.6	38.1	307.8
Kutz	P26	47.8	C15KC34B	250-300	346.8	12.8	12.8	76.5	131.1
Kutz	P26	47.8	C15KC34C	250-300	12.6	38.4	10	71.5	32.7
Kutz	P26	47.8	C15KC34D	250-300	348.7	51	9.2	79.5	138.2
Kutz	P27	48.5	C15KC35A	100, 275, 300	316.5	61.8	4.3	56.3	186.9
Kutz	P27	48.5	C15KC35D	200, 250, 275	354.4	53	9.9	84.6	131.1
Kutz	P28	56.5	C15KC36B	100-200	2.6	63	6.1	81.8	265.2
Kutz	P28	56.5	C15KC36D	NRM-150	322.6	44.2	13.1	56.6	154.4
Kutz	P29	57.8	C15KC37A	100, 200, 225	18.4	30.2	6.6	64	28.4
Kutz	P30	58.4	C15KC38A	225-275	156.1	-23	14.2	-57.4	299.4
Kutz	P30	58.4	C15KC38C	NRM, 100, 350	322.7	53.1	10.6	59.5	169.4
Kutz	P31	62.3	C15KC39A	NRM, 100, 225	328.5	67.5	5.7	63.5	203.7
Kutz	P31	62.3	C15KC39B	NRM, 100, 250	17.9	51.4	9	74.6	353.6
Kutz	P31	62.3	C15KC39D	NRM-150	45.1	57.9	9.2	54.5	324.8
Kutz	P32	66.8	C15KC41A	200, 300, 325	185.5	-26.3	15.4	-66.9	238.4
Kutz	P32	66.8	C15KC41C	125, 150, 250	84.5	-66.3	9.7	-23.3	26.4
Kutz	P32	67	C15KC42A	125-200	149.9	-68.8	5.8	-63.7	28.2
Kutz	P32	67	C15KC42C	150-225	128.9	-70.1	12	-51.1	25.5
Kutz	P32	67	C15KC42D	150-225	37.3	-69	10	-4.7	50.4
Kutz	P33	68.5	C15KC43A	200-275	122.4	-49.7	9.9	-42.3	352.5
Kutz	P33	69	C15KC44A	250-300	208.5	-62.2	15.9	-67.2	135.4
Kutz	P33	69	C15KC44C	250-300	168.2	-66.2	16.9	-75.2	40.2
Kutz	P33	69	C15KC44D	225-275	148.6	-49	8	-63	337.1
Torreon West	P22	29.4	C15TW01A	225-275	178.3	-63.2	1.3	-81.2	64.7
Torreon West	P22	29.4	C15TW01B	225-275	198.6	-61.8	3.9	-74.1	130.9
Torreon West	P22	29.4	C15TW01C	225-275	179.6	-64.4	2.7	-79.8	71
Torreon West	P24	31.5	C15TW02A	225-275	167.3	-65.8	1.7	-74.7	38.7
Torreon West	P24	31.5	C15TW02C	225-275	163.3	-55.6	3.8	-76.5	348.1
Torreon West	P24	31.5	C15TW02D	225-275	169.7	-44.9	3.3	-77.1	298.2
Torreon West	P24	31.7	C15TW03B	300, 350-375	167.4	-18.8	13.7	-61.3	279.2
Torreon West	P24	31.7	C15TW03C	225-275	195	-54	3.6	-77.7	165
Torreon West	P24	31.7	C15TW03D	225-275	172.2	-53.1	2.1	-83.2	324.8
Torreon West	P24	31.9	C15TW04A	225-275	180.3	-50.9	11.6	-85.6	249.3
Torreon West	P24	32.1	C15TW05C	225, 250, 325	171.2	-26.5	8.7	-66.6	274.6
Torreon West	P24	32.3	C15TW06A	225-275	125.6	-77.4	11.2	-46.8	43.6
Torreon West	P24	32.8	C15TW07A	125, 150, 225	167	-32.9	6.3	-68.6	288.5
Torreon West	P24	32.8	C15TW07C	225-275	147.8	-40	11	-59.2	326.1
Torreon West	P24	33.3	C15TW08A	NRM, 150, 175	170.5	-31.8	7.3	-69.4	279.2
Torreon West	P24	33.3	C15TW08B	715, 225, 275	132.9	-36.9	5.2	-46.2	335.1
Torreon West	P24	35.2	C15TW11C	200-250	219.6	-37.1	4.7	-52.3	175.6
Torreon West	P24	35.2	C15TW11D	225-275	221.4	-45.6	13.4	-53.9	165
Torreon West	P25	35.5	C15TW12B	125-275	203.9	-37.2	9.8	-64.2	192.2
Torreon West	P25	35.8	C15TW13D	100-150	38.2	72.8	6.8	56.6	288.8
Torreon West	P26	36.1	C15TW14A	125, 200, 300	174.8	-36.5	19.8	-73.7	270.2
Torreon West	P26	37.3	C15TW15B	225-275	1	20.8	7	64.7	70.3
Torreon West	P26	38.2	C15TW16D	125, 250, 225	296.2	51.7	13.2	38	178.3
Torreon West	P26	39	C15TW17B	150, 200, 250	353.6	45.1	17.5	79.2	104.6
Torreon West	P27	40	C15TW18C	150, 200, 225	12.3	31.5	9.4	68.1	39.5
Torreon West	P29	43.2	C15TW19A	100, 125, 175	8	39.2	4.8	74.5	43.7
Torreon West	P29	43.2	C15TW19B	100-150	342.2	59.7	4	75.3	186
Torreon West	P29	43.2	C15TW19C	225-275	309.9	48.7	9.9	47.9	168.8
Torreon West	P39	56.7	C15TW20A	225-275	355.2	63.6	1.5	80.1	232.5
Torreon West	P39	56.7	C15TW20C	225-275	358.7	60	3.4	85	241.2
Torreon West	P39	56.7	C15TW20D	225-275	359.6	66.5	3	77	251.4
Torreon West	P40	61.4	C15TW21A	125, 175, 200	16	52.7	3.9	76.6	349.6
Torreon West	P40	61.4	C15TW21B	225-275	353.2	58	8.8	84	190.9
Torreon West	P40	61.4	C15TW21C	175-225	296	72.5	5.2	43.3	211.4
Torreon West	P43	66.7	C15TW22A	225-275	0.2	80.5	5	54.5	252.7
Torreon West	P43	66.7	C15TW22B	125, 150, 225	350	55.7	1	81.9	167.3
Torreon West	P43	66.7	C15TW22D	175-225	341.2	50	4.1	73.5	149.6
Torreon West	P49	72	C15TW23A	125, 250, 275	5.2	43.3	2.4	78.3	48.7
Torreon West	P49	72	C15TW23C	100-150	355.2	42.8	4.1	78.1	94.2
Torreon West	P49	72	C15TW23D	100-150	349.6	67.3	4.5	74	227.7
Torreon West	P49	72.4	C15TW24A	100-150	5.2	-74.6	4.8	-7.2	70.1
Torreon West	P50	72.7	C15TW25C	225-275	131	-49.5	13.4	-49	349.3
Torreon West	P50	73.3	C15TW27D	125, 275, 200	152.8	-75.2	15.3	-58.9	48.2
Torreon West	P50	73.8	C15TW28A	175, 200, 250	230.1	-51.2	10.1	-48.7	153.3
Torreon West	P50	73.8	C15TW28B	175, 275, 325	302.4	-79.7	19.9	-23.9	91
Torreon West	P50	74	C15TW29B	100-150	160.3	-42.9	10.7	-69.8	314.8
Torreon West	P51	74.6	C15TW30A	250, 275, 325	196.7	-36.8	14.2	-68.7	204.8
Torreon West	P51	74.6	C15TW30B	175-225	7.5	73.5	8.4	66.1	262.1
Torreon West	P52	75.9	C15TW32A	300, 325, 375	173.2	-25.7	18.4	-66.7	269.5
Torreon West	P52	76.8	C15TW36C	150-200	149.1	-48.9	15.6	-63.5	338.1
Torreon West	P53	77.4	C15TW37B	225-275	170.4	-28.6	7.2	-67.5	277.5

APPENDIX 1
(continued)

Location	Paleosol #	Strat level (m)	Sample	Temp. steps	Strat. Declination	Strat. Inclination	MAD	Strat. VGP latitude	Strat. VGP longitude
Torreon West	P53	77.4	C15TW37C	250, 275, 325	140.2	-36.6	17.8	-51.9	329.3
Torreon West	P53	77.4	C15TW37D	200-250	168.6	-59.2	8.1	-80.2	10
Torreon West	P53	78.4	C15TW38B	125, 300, 325	119.5	-25.1	5	-31.5	336
Torreon West	P53	78.4	C15TW38C	225, 250, 300	128.7	-51.9	19.2	-47.9	353.4
Torreon East	P7	27.5	C15ET02A	175-225	153.3	-43	6.8	-64.6	324.5
Torreon East	P7	27.8	C15ET03A	NRM-125	203.5	-47.7	8.3	-69	176
Torreon East	P7B	27.8	C15ET03B	200, 250, 275	142.4	-64.5	7.4	-60.2	14.8
Torreon East	P7	27.8	C15ET03D	150, 200, 250	233.4	-76.9	9	-47.4	102.7
Torreon East	P7	28	C15ET04A	275-325	144.3	-24.4	7.3	-50.4	316
Torreon East	P7	28	C15ET04B	200-250	121.4	-50.7	10.4	-41.8	355.1
Torreon East	P7	28.5	C15ET05C	125-175	124.6	-37.8	11.5	-39.9	341.3
Torreon East	P8	29.8	C15ET07A	225-275	208.1	-68.3	9.4	-64.7	116.1
Torreon East	P8	29.8	C15ET07B	125-175	117.8	-41.5	10	-35.7	348.1
Torreon East	P8	29.8	C15ET07C	125, 175, 275	154.9	-54.8	15.3	-69.7	348.2
Torreon East	P9	31.5	C15ET11D	225, 250, 300	105	-38.8	12.9	-24.4	352.9
Torreon East	P10	32	C15ET12A	225-275	9.6	80.2	1	54.7	258.1
Torreon East	P10	32	C15ET12B	100-150	12.9	46	4.9	76.1	17.3
Torreon East	P10	32	C15ET12D	150, 300, 325	220.4	70.6	0.6	7.2	230.6
Torreon East	OVBK	32.5	C15ET13A	125-175	261.9	85.8	1.2	34.4	242.7
Torreon East	OVBK	32.5	C15ET13B	100, 125, 200	170.4	75	4.5	8.1	257.3
Torreon East	OVBK	32.5	C15ET13C	100-150	200.1	76.5	3.5	11.6	244
Torreon East	P11	33	C15ET14B	100-150	355.4	30.6	13.2	70	85.7
Torreon East	P11	33	C15ET14C	100-150	59.1	50.4	17.4	41.3	330.4
Torreon East	P11	33	C15ET14D	175-225	4.2	50.9	7.4	84.4	33.1
Torreon East	P12	35	C15ET16C	NRM-150	44.3	70.5	14.4	54.5	296.8
Torreon East	P17	46	C15ET44A	200-250	340.9	64.1	12.3	72.6	203
Torreon East	P17	46	C15ET44C	100-150	353.7	69.8	12.2	71.8	240.7
Torreon East	P17	48	C15ET43B	100-150	250.6	72.8	7.9	21	220.6
Torreon East	P17	48	C15ET43C	150-200	350.5	68.6	7.9	72.7	232.7
Torreon East	P17	48	C15ET43D	NRM-125	41.7	60.6	3.5	57.3	319.9
Torreon East	P17	50	C15ET42B	NRM-125	51.9	74.5	16.5	49.1	288.4
Torreon East	P17	50	C15ET42C	150, 175, 225	345.1	36.4	10.2	69.5	116.3
Torreon East	P17	50	C15ET42D	150-200	335.6	61.5	12	70.1	189.6
Torreon East	P19	55	C15ET41C	NRM-125	340.5	76	13.7	60	235.3
Torreon East	P19	55	C15ET41D	150, 175, 225	346.2	63.7	7.7	76	208.8
Torreon East	P19	55.5	C15ET17A	125-175	332.9	24.5	3.7	56.4	126.1
Torreon East	P19	55.5	C15ET17B	100, 225, 275	353.6	21.9	4.3	64.7	87.5
Torreon East	P19	57	C15ET40A	125, 150, 200	331.1	65.2	6.2	65.8	199.4
Torreon East	P19	57	C15ET40B	100-150	354.3	65.8	3.5	77.2	235.2
Torreon East	P19	57	C15ET40C	125, 150, 275	326.4	67.1	5.7	62.1	202.9
Torreon East	P20	58	C15ET18C	225, 275, 300	110.2	-33	13.9	-26.6	346.3
Torreon East	P21	60	C15ET39C	225-275	191.3	-69.5	8.2	-71.1	93.9
Torreon East	P21	60	C15ET39D	250-300	33.1	-81.4	18.2	-21.5	62.9
Torreon East	P22	61	C15ET38A	150, 175, 275	168.5	-15.4	9.5	-59.9	275.9
Torreon East	P22	61	C15ET38C	NRM, 100, 175	164	-36.2	6.1	-68.8	298.4
Torreon East	P22	61	C15ET38D	250-300	189.3	-32.3	0.8	-69.8	226.2
Torreon East	P22	61.5	C15ET37B	175, 200, 275	172.8	-46	2.7	-79.4	290
Torreon East	P22	61.5	C15ET37C	NRM-125	181.6	-60.1	11.5	-84.8	86.2
Torreon East	P22	61.5	C15ET37D	200, 250, 275	143.4	-60	4.3	-61.1	3.7
Torreon East	SS10	61.8	C15ET36A	175, 225, 250	173.2	-50.3	15.7	-82.5	303.5
Torreon East	SS10	61.8	C15ET36B	125-175	171.7	-20.3	13.8	-63.4	271.2
Torreon East	SS10	61.8	C15ET36D	175, 200, 275	162.1	-40.9	4.4	-70.1	308.5
Torreon East	P23	62	C15ET19A	200, 225, 300	214.8	-40.4	4	-57.3	176.3
Torreon East	P23	62	C15ET19C	200-250	141.2	-78	13	-52	49.3
Torreon East	P23	63	C15ET21A	200, 250, 275	135	-39.8	13.6	-48.9	336.4
Torreon East	P23	63	C15ET21B	225-275	145	-68.1	13.3	-60.8	25.2
Torreon East	P23	63	C15ET21D	125-175	141.2	-78	7.3	-55.1	345.7
Torreon East	P23	63.5	C15ET22A	125-175	171.8	-29.6	7.6	-68.6	274.8
Torreon East	P23	63.5	C15ET22B	125, 150, 250	191.5	-45.6	15.9	-76.7	202
Torreon East	P23	63.5	C15ET22D	200, 225, 275	169.3	-34.4	11.9	-70.5	284.4
Torreon East	P23	64	C15ET23A	150, 175, 300	182.1	-48.8	7.7	-83.5	236.4
Torreon East	P23	64	C15ET23B	250-300	164.3	-33.3	11.4	-67.4	294.7
Torreon East	P23	64.5	C15ET24B	225-275	205.4	-61.7	6.2	-69.3	135.5
Torreon East	P23	64.5	C15ET24C	225-275	218.9	-64.3	4.5	-59.3	131.3
Torreon East	P23	64.5	C15ET24D	225-275	204	-61.7	7.1	-70.3	134.9
Torreon East	P23	65	C15ET25B	100, 125, 175	187.7	-50.9	8.9	-82.2	195
Torreon East	P23	65	C15ET25C	250-300	143.6	-49.4	12.4	-59.2	342.6
Torreon East	P23	65	C15ET25D	125, 225, 250	170.3	-63.3	6.4	-78.5	35.9
Torreon East	P24	65.2	C15ET26A	125-175	175	-57.8	10.2	-85.3	15.8
Torreon East	P24	65.2	C15ET26B	150, 250, 300	176.2	-36.8	3.7	-74.2	265.8
Torreon East	P24	65.2	C15ET26C	125-175	203	-46.6	5.7	-68.9	178.9
Torreon East	P24	65.8	C15ET27A	150-200	155.6	-59.3	12.5	-70.4	2.2
Torreon East	P24	65.8	C15ET27C	225-275	214.8	-79.7	2.7	-51.2	90.8
Torreon East	P24	65.8	C15ET27D	250-300	174.8	-82.5	3	-50.7	70.6

APPENDIX 1
(continued)

Location	Paleosol #	Strat level (m)	Sample	Temp. steps	Strat. Declination	Strat. Inclination	MAD	Strat. VGP latitude	Strat. VGP longitude
Torreon East	P24	66.3	C15ET28B	225-275	155.4	-42.8	7.3	-66.1	321.7
Torreon East	P24	66.3	C15ET28C	150, 175, 250	158.3	-33	5.4	-63.7	305.2
Torreon East	P24	66.3	C15ET28D	150-200	119.4	-42	4.4	-37.1	347.7
Torreon East	P24	66.8	C15ET30A	125-175	124.7	-52	16.1	-44.8	355.3
Torreon East	P24	66.8	C15ET30B	200-250	131.3	-60	8.7	-52	5.3
Torreon East	P24	66.8	C15ET30D	125-175	139.8	-30	14.6	-49.2	324.2
Torreon East	P24	67	C15ET31A	150-200	129.1	-65.6	7.5	-51.1	16.6
Torreon East	P24	67	C15ET31C	150, 175, 250	154.8	-46	20.4	-67	327.8
Torreon East	P24	67	C15ET31D	150-200	134.9	-53.5	9.1	-53.3	353.2
Torreon East	P25	70	C15ET32A	225-275	172.6	-67.3	4.8	-74.9	54.2
Torreon East	P25	70	C15ET32C	225-275	147.3	-55	5.9	-63.6	351.4
Torreon East	P25	70	C15ET32D	225-275	157.5	-57.9	4.2	-72	357.6
Torreon East	P26	71.5	C15ET33A	225-275	163.2	-62.6	4	-74.9	19.7
Torreon East	P26	71.5	C15ET33B	225-275	139.6	-57.4	4.2	-57.9	358.6
Torreon East	P26	71.5	C15ET33D	150-200	155.8	-58.3	8.6	-70.6	358.9
Torreon East	P26	72.5	C15ET34A	175, 275, 300	101.8	-72.6	8.9	-35.9	32.8
Torreon East	P26	72.5	C15ET34B	175, 200, 250	103.4	-62.2	6.5	-32.7	15.7
Torreon East	P26	72.5	C15ET34D	175, 200, 250	100	-66.2	5.4	-32.3	22.3
Torreon East	ss13m	74	C15ET35B	150, 175, 225	192.6	-29.8	3.4	-67	220.2
Torreon East	ss13m	74	C15ET35C	200-250	157	-66.1	6.8	-69	26.3
Escavada Wash	P1	1	C15EM01A	100, 150, 175	213.5	-49.6	4.2	-61.6	164.1
Escavada Wash	P1	1	C15EM01B	125-175	233.2	-67.9	7.6	-49.6	123.8
Escavada Wash	P2	2.6	C15EM02B	150-200	155.6	-25.9	15.1	-58.7	303.2
Escavada Wash	P3	4.3	C15EM03B	225, 275, 300	118.4	-55.8	3.9	-41.2	2.3
Escavada Wash	P3	4.3	C15EM03C	200-250	122.1	-58.7	4	-44.9	5.2
Escavada Wash	P3	4.3	C15EM04B	275-325	109.1	-43.9	4.3	-29.6	354.4
Escavada Wash	P5	5.9	C15EM04B	275-325	149	-64.3	4.4	-64.7	15.8
Escavada Wash	P5	5.9	C15EM04C	150-200	133.1	-53.3	4.8	-51.9	353.5
Escavada Wash	P5	5.9	C15EM04D	250-300	156.9	-52.3	4.8	-70.7	340.1
Escavada Wash	P8	7.2	C15EM05B	275-325	142.8	-26.4	6.2	-50.1	318.7
Escavada Wash	P8	7.2	C15EM05D	275-325	167.4	-26.9	4.3	-65.5	283.2
Escavada Wash	SS05	8.5	C15EM06B	275-325	112.1	-40.6	10.7	-30.8	350.3
Escavada Wash	SS05	8.5	C15EM06D	350-400	181.1	-19	16.7	-63.7	250.2
Escavada Wash	SS06	10	C15EM07B	125-175	1.2	50.7	4.7	85.3	60
Escavada Wash	SS06	10	C15EM07C	125-175	19.6	49	2.9	72.5	357.4
Escavada Wash	SS06	10	C15EM07D	225-275	347.3	66.2	2.1	74.3	220
Escavada Wash	P9	12.5	C15EM08A	275-325	183.9	-60.4	2.1	-83.8	101
Escavada Wash	P9	12.5	C15EM08C	275-325	150.8	-68.3	6.1	-64.1	28.5
Escavada Wash	P9	12.5	C15EM08D	275-325	161.1	-65.9	5.8	-71.5	29.7
Escavada Wash	SS07	13. 8	C15EM09A	275-325	173.9	-53.6	7.5	-84.7	324
Escavada Wash	SS07	13.8	C15EM09B	275-325	160.9	-54.1	2.3	-74.4	343.2
Escavada Wash	SS07	13.8	C15EM09C	225-275	149.9	-47.6	1.8	-63.7	335.2
Escavada Wash	P10	15	C15EM10A	275-325	134.7	-47.8	6	-75.3	318
Escavada Wash	P10	15	C15EM10C	200-250	196.3	-62.1	4.5	-75.5	127.2
Escavada Wash	P10	15	C15EM10D	250-300	180.2	-39.6	5.1	-76.5	251.8
Escavada Wash	P11	16.6	C15EM11A	250-300	184.8	-28.9	4.2	-69	239.6
Escavada Wash	P11	16.6	C15EM11C	250-300	139.7	-48.4	4.7	-55.7	343.2
Escavada Wash	P11	16.6	C15EM11D	225, 300, 325	169.4	-24.4	11	-64.9	277.6
Escavada Wash	P14	17.6	C15EM12A	150-200	183.1	-25.4	13.2	-67.2	244.8
Escavada Wash	P18	19.1	C15EM13A	250-300	173	-53	5	-83.8	321.7
Escavada Wash	P18	19.1	C15EM13B	200-250	159.6	-46.9	1.8	-71	323.8
Escavada Wash	P18	19.1	C15EM13D	275-325	146.4	-58.7	2.2	-63.4	0.2
Escavada Wash	P19	20.5	C15EM14A	225-275	164.5	-61.4	4.1	-76.4	15.9
Escavada Wash	P19	20.5	C15EM14B	275-325	175.2	-34.5	6	-72.4	267.8
Escavada Wash	P19	20.5	C15EM14C	275-325	171.8	-26.4	7.2	-66.7	273.1
Escavada Wash	P21	22	C15EM15B	275-325	189.9	-48.4	2.8	-79.4	198.3
Escavada Wash	P21	22	C15EM15C	225-275	149.2	-63.3	6.5	-65.1	12.9
Escavada Wash	P21	22	C15EM15D	250-300	179.7	-67.1	4.3	-76.2	71.8
Escavada Wash	P24	23.5	C15EM16A	100-150	140.3	-22.6	7.6	-46.8	318.6
Escavada Wash	P24	23.5	C15EM16C	125-175	171.5	-64.6	2.8	-77.7	44
Escavada Wash	P24	23.5	C15EM16D	125-175	151.9	-34	7	-59.8	315.1
Escavada Wash	P26	30.9	C15EM18C	225-275	158.7	-28	13	-61.6	300.1
Escavada Wash	P27	32.3	C15EM19A	250-300	215.6	-66.1	2.2	-61.2	125.8
Escavada Wash	P27	32.3	C15EM19B	250-300	161.5	-38.4	7	-68.4	305.9
Escavada Wash	P27	32.3	C15EM19D	150, 200, 275	225.1	-57.4	6.3	-54.3	145.5
Escavada Wash	P29	34	C15EM20B	275-325	166.8	-45.3	5.6	-75.5	307
Escavada Wash	P29	34	C15EM20C	275-325	154.1	-49.8	4.8	-67.8	336.1
Escavada Wash	SS12	42	C15EM21A	175-225	329.7	50.6	5	64.5	160.9
Escavada Wash	SS12	42	C15EM21B	100, 125, 200	325.4	46.4	5.5	59.6	156.7
Escavada Wash	SS12	42	C15EM21C	100-150	335.7	27.4	6	59.5	124.2
Escavada Wash	SS12	43.3	C15EM22B	100-150	346.4	56.7	4.9	79	173.3
Escavada Wash	SS12	43.3	C15EM22C	100-150	322.5	51.3	3.5	58.8	166.2
Escavada Wash	SS12	43.3	C15EM22D	100-150	341.3	46.2	2.2	72	139.8

APPENDIX 1
(continued)

Location	Paleosol #	Strat level (m)	Sample	Temp. steps	Strat. Declination	Strat. Inclination	MAD	Strat. VGP latitude	Strat. VGP longitude
Escavada Wash	P30	45	C15EM23B	100-150	330.5	49.3	8.6	64.7	157.8
Escavada Wash	P30	45	C15EM23C	100-150	310.6	54.7	5.3	50.3	176.6
Escavada Wash	P30	46.3	C15EM24A	150-200	360	18.1	4.7	63.3	72.6
Escavada Wash	P31	48	C15EM25B	125, 200, 250	42.1	58.3	9.2	56.8	324.5
Escavada Wash	P32	49.5	C15EM26A	275-325	327.3	38.7	2.8	58.3	145.1
Escavada Wash	SS13	51	C15EM27A	250-300	28.1	48.6	3.8	65.6	349.8
Escavada Wash	SS13	51	C15EM27B	250-300	7.7	39.5	4.3	74.8	44.3
Escavada Wash	SS13	51	C15EM27C	100-150	315.7	63.4	7.3	55.6	191.6
Escavada Wash	P33	52.5	C15EM28A	100, 125, 175	3.9	43.9	9.3	79.2	53.6
Escavada Wash	P33	52.5	C15EM28B	NRM-125	17	68.7	15.1	69.9	284.2
Escavada Wash	P33	52.5	C15EM28D	100-150	351.6	43.2	15.2	77	108.5
Escavada Wash	P33	54	C15EM29C	100-150	25.8	47.5	4.4	67.1	354
Escavada Wash	P33	54	C15EM29D	125, 150, 200	12.1	70.7	18.3	69.3	272.5
Escavada Wash	P35	55.5	C15EM30A	NRM-125	23.8	26.4	7.1	59.3	22.5
Escavada Wash	P35	55.5	C15EM30C	150, 200, 225	28.7	28.2	5.4	56.9	14.5
Escavada Wash	P37	57	C15EM31B	NRM-125	350.1	23.9	4	64.9	95.9
Escavada Wash	P37	57	C15EM31C	NRM, 100, 200	336.7	27.6	5.1	60.2	122.9
Escavada Wash	P37	57	C15EM31D	NRM, 100, 250	16.9	43.6	9.7	72.1	14
Escavada Wash	P39	58.5	C15EM32A	275-325	353.6	69.3	2.9	72.5	239.7
Escavada Wash	P39	58.5	C15EM32C	NRM, 125, 175	324	29.2	6.1	52.1	139.6
Escavada Wash	P39	58.5	C15EM32D	125-175	343.9	48.1	3.8	74.8	140.3
Escavada Wash	P40	59.5	C15EM33A	150-200	20.8	55.2	7.3	73.2	337.4
Escavada Wash	P40	59.5	C15EM33B	150-200	354.5	66.5	3.5	76.4	237.1
Escavada Wash	P40	59.5	C15EM33C	150-200	355.9	62.3	2.5	81.8	231.4
Escavada Wash	P42	59	C15EM34A	NRM, 100, 150	309.2	52	6.9	48.4	173.3
Escavada Wash	P42	59	C15EM34B	NRM, 100, 150	333.8	54.3	4.8	68.7	167.2
Escavada Wash	P42	59	C15EM34D	NRM-125	317.4	62.2	7.8	56.8	188.9
Escavada Wash	SS15	59.5	C15EM35A	225-275	351.4	64.9	1	77.4	224.7
Escavada Wash	SS15	59.5	C15EM35B	125-175	348.9	60.4	2.9	79.8	197.7
Escavada Wash	SS15	59.5	C15EM35D	200-250	357	62.6	3.8	81.7	237.5
Escavada Wash	SS15	59.8	C15EM36B	100-150	338.4	67	7.4	69.2	210.4
Escavada Wash	SS15	59.8	C15EM36D	100-150	340.7	59.7	2.5	74.2	185.2
Escavada Wash	SS16	61.5	C15EM37A	NRM-125	355.9	21.2	13.3	64.7	82.1
Escavada Wash	SS16	61.5	C15EM37B	NRM-125	358.4	38.6	4	75.7	78.6
Escavada Wash	SS16	61.5	C15EM37D	NRM-125	346	44.6	7.4	74.6	127.3
Escavada Wash	P45	63	C15EM38B	NRM-125	348.4	41.7	4.4	74.4	115.6
Escavada Wash	P45	63	C15EM38C	100-150	359.9	53.1	5	87.7	74.6
Escavada Wash	P45	63	C15EM38D	100-150	356.1	30.4	4.9	70	83.6
Escavada Wash	P47	64.5	C15EM39B	200-250	16.2	59.5	5.8	76.6	318.9
Escavada Wash	P47	64.5	C15EM39C	100-150	353.7	49.3	5.5	82.1	116.5
Escavada Wash	P47	64.5	C15EM39D	200-250	354.7	59.6	3.4	83.9	211
Escavada Wash	P47	66	C15EM40A	100-150	8.8	44.4	4.9	77.6	33
Escavada Wash	P47	66	C15EM40B	100, 175, 200	32.4	65	6.8	63.6	307.9
Escavada Wash	P47	66	C15EM40C	NRM-125	83.6	68.3	6	31.1	298.9
Escavada Wash	P48	67.5	C15EM41A	125-175	194.8	86.1	4.2	28.5	250.4
Escavada Wash	P48	67.5	C15EM41B	225, 275, 300	179.6	87.6	12	31.2	252.6
Escavada Wash	P48	67.5	C15EM41D	125, 150, 200	276.6	81.5	7.1	36.1	232
Escavada Wash	P48	69	C15EM42A	NRM, 150, 175	349	75	3.6	63.3	241
Escavada Wash	P48	69	C15EM42C	125-175	308.4	34.4	2.7	41.7	156.2
Escavada Wash	SS21	75.5	C15EM45B	100-150	153.6	-50.3	2.7	-67.5	337.6
Escavada Wash	SS21	75.5	C15EM45C	200, 250, 275	146.2	-52.9	15.8	-62.2	347.4
Escavada Wash	SS21	75.5	C15EM45D	225-275	164.3	-48.7	3.5	-75.4	321.3
Escavada Wash	P52	78	C15EM46B	225-275	207	-77.8	5.9	-55.6	91.2
Escavada Wash	P52	79	C15EM47A	225-275	159.5	-53.5	7.4	-73.1	342
Escavada Wash	P52	79	C15EM47B	150-200	200.3	-59.1	7.7	-73.5	141.7
Escavada Wash	P52	79	C15EM47D	250-300	169.9	-60	15	-80.7	17.4
Escavada Wash	P53	81	C15EM48B	125-175	192	-60.7	12.1	-79.1	127.5
Escavada Wash	P53	81	C15EM48C	100-150	152.4	-57.1	5.3	-67.9	355.3
Escavada Wash	P53	81	C15EM48D	100, 150, 175	155.1	-56.3	7.7	-70	352.5
Escavada Wash	P54	82	C15EM49A	200, 250, 275	191	-78.7	3.7	-57.2	80.1
Escavada Wash	P54	82	C15EM49C	150-200	207.3	-50.2	4.8	-66.8	167.2
Escavada Wash	P54	82	C15EM49D	100-150	229.4	-41.9	16.5	-46.1	164.1
Escavada Wash	P56	84	C15EM50A	150-250	167.4	-57.2	16.7	-79.8	356.5
Escavada Wash	P56	84	C15EM50C	125, 150, 200	207.6	-55.2	7.7	-67.7	155.1

APPENDIX 2

Paleomagnetic data: site means

Location	Paleosol #	Strat level (m)	Sample #	n*	Strat. Declination	Strat. Inclination	alpha-95	Strat. VGP latitude	Strat. VGP longitude
Kutz	P37	4.5	C15KC48	3	153.7	-67.9	17.1	-66.4	28
Kutz	P5	21.75	C15KC7	3	160.5	-36	26.2	-066.2	303.3
Kutz	P7	26.5	C15KC10	3	188.6	-26.4	14.2	-66.2	231.1
Kutz	P9	27.5	C15KC12	3	180.1	-44.5	6.3	-79.7	251.6
Kutz	P11	30.5	C15KC16	3	351.8	62	24.7	80.8	211.6
Kutz	P12	31.5	C15KC17	3	347.3	38.5	32.3	71.5	112.3
Kutz	P13	32.5	C15KC18	3	1.6	62.9	11.4	82.1	260.4
Kutz	P13	32.75	C15KC19	3	2.9	51.2	19.2	84.8	43.9
Kutz	P14	33.5	C15KC20	3	359	52.9	12.5	86.9	87.5
Kutz	P16	36.5	C15KC24	3	6	50	13	82.4	29.2
Kutz	P24	46	C15KC32	3	357.1	68.9	14.3	74	245.7
Kutz	P26	47.8	C15KC34	3	357	46.3	18.7	80.8	88.9
Kutz	P31	62.25	C15KC39	3	15.9	62.1	30.4	76	307.8
Kutz	P32	67	C15KC42	3	110	-75.9	29.3	-40.9	38.2
Kutz	P33	69	C15KC44	3	171.6	-61.6	27.9	-81	28.8
Escavada Wash	P3	4.3	P16EM03	3	115.8	-52.9	13.6	-38.2	359.8
Escavada Wash	P5	5.9	P16EM04	3	146.2	-57.1	14.7	-63	356.4
Escavada Wash	SS06	10	P16EM07	3	5	55.9	19.9	85.9	334.8
Escavada Wash	P9	12.5	P16EM08	3	167	-65.5	12.7	-74.9	37.1
Escavada Wash	SS07	13.75	P16EM09	3	161	-52.2	12.7	-74	336.6
Escavada Wash	P10	15	P16EM10	3	168.5	-52.6	35.7	-80.1	329.4
Escavada Wash	P11	16.6	P16EM11	3	167	-35.2	34.6	-69.9	290.7
Escavada Wash	P18	19.1	P16EM13	3	160.2	-53.3	14.9	-73.7	340.9
Escavada Wash	P19	20.5	P16EM14	3	171.5	-40.7	29.2	-75.3	284.9
Escavada Wash	P21	22	P16EM15	3	175.3	-60.8	22.3	-83.1	41.9
Escavada Wash	SS12	42	P16EM21	3	330.8	41.6	20	62.1	145.1
Escavada Wash	SS12	43.3	P16EM22	3	336.5	51.8	14.3	70.3	159
Escavada Wash	P33	52.5	P16EM28	3	1.6	52.3	25	86.6	49.1
Escavada Wash	P37	57	P16EM31	3	353	32.7	30.8	70.8	93.2
Escavada Wash	P39	58.5	P16EM32	3	336.5	49.5	35.1	69.6	153.3
Escavada Wash	P42	59	P16EM34	3	320.1	56.6	13.7	58.2	176.8
Escavada Wash	P40	59.5	P16EM33	3	5.4	61.9	14.2	81.8	281.2
Escavada Wash	SS15	59.5	P16EM35	3	352.4	62.7	4.5	80	219.3
Escavada Wash	SS16	61.5	P16EM37	3	353.8	34.9	20.4	72.4	92.3
Escavada Wash	P45	63	P16EM38	3	354.5	41.8	18.6	77.2	95.8
Escavada Wash	P47	64.5	P16EM39	3	0.8	56.6	13.9	88.7	281.1
Escavada Wash	P47	66	P16EM40	3	32.5	62.7	34.8	64	314.4
Escavada Wash	P48	67.5	P16EM41	3	241.4	86.4	8	32.3	245.1
Escavada Wash	SS21	75.5	P16EM45	3	154.9	-50.8	9.4	-68.7	337.7
Escavada Wash	P52	79	P16EM47	3	175.6	-58.7	18.1	-85.1	28.5
Escavada Wash	P53	81	P16EM48	3	165.4	-59.2	17.7	-77.8	6.1
Escavada Wash	P54	82	P16EM49	3	215.7	-57.6	33.5	-61.6	147.3
Torreon West	P22	29.4	C15TW01	3	185.8	-63.4	8.1	-80	97
Torreon West	P24	31.5	C15TW02	3	167	-55.5	16.3	-79.5	346.6
Torreon West	P29	43.2	C15TW19	3	341.7	51.9	34.6	74.5	155
Torreon West	P39	56.7	C15TW20	3	357.8	63.4	5.2	80.9	242.7
Torreon West	P40	61.4	C15TW21	3	352.4	64.3	30.8	78.4	225.4
Torreon West	P43	66.7	C15TW22	3	347.1	62.1	25.8	77.7	203.2
Torreon West	P49	72	C15TW23	3	358	51.2	22.8	85.6	95.1
Torreon West	P53	77.4	C15TW37	3	159	-42.3	32.1	-68.6	315.8
Torreon East	P7	27.75	C15ET03	3	189.7	-67	34.2	-74.6	97
Torreon East	P19	57	C15ET40	3	337.3	66.5	9.3	69	207.9
Torreon East	P22	61	C15ET38	3	173.8	-28.4	24.9	-68.4	269.2
Torreon East	P22	61.5	C15ET37	3	166.8	-56.4	20.6	-79.4	351.8
Torreon East	SS10	61.75	C15ET36	3	169	-37.3	24.9	-72.1	288.1
Torreon East	P23	63	C15ET21	3	138.4	-52.5	22.6	-55.9	350.2
Torreon East	P23	63.5	C15ET22	3	176.7	-36.9	19.2	-74.3	264.2
Torreon East	P23	64.5	C15ET24	3	209.1	-62.7	6.1	-66.4	133.7
Torreon East	P23	65	C15ET25	3	166.6	-56	23.8	-79.2	349.6
Torreon East	P24	65.2	C15ET26	3	184.9	-47.8	23.2	-81.8	221.2
Torreon East	P24	65.75	C15ET27	3	170.7	-75.2	23	-63.2	63.1
Torreon East	P24	66.25	C15ET28	3	145.1	-40.6	27	-57.3	329.4
Torreon East	P24	66.75	C15ET30	3	133	-47.6	25.5	-50	346
Torreon East	P24	67	C15ET31	3	141.6	-55.5	19.4	-59.1	354.3
Torreon East	P25	70	C15ET32	3	157.5	-60.4	13.5	-71.7	6.5
Torreon East	P26	71.5	C15ET33	3	152.3	-59.8	10.2	-67.9	3.3
Torreon East	P26	72.5	C15ET34	3	101.8	-67	8.1	-33.7	23.1

APPENDIX 3

Summary of $^{40}Ar/^{39}Ar$ Results

ID	Power (watts)	$^{40}Ar/^{39}Ar$	$^{37}Ar/^{39}Ar$	$^{36}Ar/^{39}Ar$ (x 10^{-3})	$^{39}Ar_K$ (x10^{-15} mol)	K/Ca	$^{40}Ar^*$ (%)	Age (Ma)	±1σ (Ma)
H16-SJ-11, Detrital Sanidine, J=0.0018728±0.03%, IC=1.010695±0.0017517, NM-291D, Lab#=65815, Argus VI									
39	4.5	18.96	0.0162	1.725	0.309	31.5	97.3	62.16	0.12
65	4.5	18.60	0.0045	0.4969	0.794	113.3	99.2	62.174	0.047
83	4.5	18.84	0.0110	1.252	0.819	46.3	98.0	62.231	0.048
44	4.5	18.64	0.0032	0.5331	0.926	158.8	99.2	62.269	0.041
80	4.5	18.58	0.0056	0.3124	0.986	91.0	99.5	62.272	0.039
46	4.5	18.66	0.0052	0.5740	0.920	98.6	99.1	62.280	0.041
08	4.5	18.70	0.0088	0.7001	0.861	58.2	98.9	62.286	0.043
79	4.5	18.57	0.0072	0.2567	1.423	71.3	99.6	62.290	0.029
72	4.5	18.66	0.0055	0.5750	0.699	92.1	99.1	62.300	0.052
85	4.5	18.69	0.0045	0.6524	0.846	113.1	99.0	62.311	0.045
06	4.5	18.73	0.0051	0.7722	1.257	99.7	98.8	62.340	0.032
61	4.5	18.70	0.0098	0.6443	0.907	52.0	99.0	62.342	0.041
04	4.5	18.84	0.0060	1.122	1.524	85.0	98.2	62.348	0.028
09	4.5	18.60	0.0066	0.3011	1.438	77.2	99.5	62.356	0.029
07	4.5	19.52	0.0055	3.361	0.802	93.5	94.9	62.394	0.050
27	4.5	19.23	0.0115	2.397	0.592	44.5	96.3	62.399	0.066
17	4.5	19.07	0.0045	1.853	1.214	114.6	97.1	62.400	0.034
05	4.5	18.72	0.0046	0.6558	1.235	109.9	99.0	62.411	0.032
03	4.5	18.62	0.0052	0.3196	2.411	98.7	99.5	62.414	0.018
32	4.5	18.70	0.0073	0.5564	1.063	70.3	99.1	62.426	0.036
52	4.5	18.76	0.0045	0.7667	0.577	114.5	98.8	62.427	0.061
31	4.5	18.79	0.0089	0.8474	0.535	57.0	98.7	62.435	0.072
24	4.5	18.62	0.0048	0.2894	1.283	106.8	99.5	62.439	0.030
35	4.5	18.61	0.0071	0.2380	1.160	71.8	99.6	62.444	0.031
77	4.5	18.60	0.0052	0.2157	1.745	98.5	99.7	62.446	0.023
87	4.5	18.61	0.0061	0.2470	1.430	84.1	99.6	62.449	0.027
54	4.5	18.73	0.0058	0.6516	0.903	88.4	99.0	62.456	0.042
64	4.5	18.63	0.0046	0.2954	2.033	111.1	99.5	62.456	0.020
67	4.5	18.72	0.0100	0.6020	1.038	50.8	99.1	62.459	0.039
88	4.5	18.73	0.0111	0.6328	0.883	45.9	99.0	62.462	0.043
66	4.5	18.78	0.0052	0.7859	1.447	97.5	98.8	62.464	0.027
59	4.5	18.68	0.0065	0.4706	1.032	78.4	99.3	62.468	0.039
71	4.5	18.67	0.0076	0.4394	0.986	67.3	99.3	62.469	0.040
43	4.5	18.77	0.0037	0.7539	1.056	137.2	98.8	62.475	0.037
56	4.5	18.91	0.0108	1.214	0.543	47.2	98.1	62.484	0.068
26	4.5	18.67	0.0055	0.4128	2.265	92.6	99.3	62.484	0.019
78	4.5	18.70	0.0053	0.5131	1.087	95.5	99.2	62.487	0.038
12	4.5	18.69	0.0031	0.4843	1.988	164.7	99.2	62.490	0.021
74	4.5	18.69	0.0040	0.4660	1.423	126.1	99.3	62.490	0.028
23	4.5	18.75	0.0041	0.6532	1.549	124.3	99.0	62.494	0.027
33	4.5	18.69	0.0051	0.4473	1.920	100.7	99.3	62.496	0.021
19	4.5	18.73	0.0072	0.6112	0.991	71.1	99.0	62.500	0.039
29	4.5	18.67	0.0032	0.3961	1.452	158.1	99.4	62.500	0.027
25	4.5	18.78	0.0048	0.7506	2.293	106.6	98.8	62.501	0.019
53	4.5	18.73	0.0057	0.5935	1.160	89.5	99.1	62.502	0.034
82	4.5	18.82	0.0058	0.9105	1.509	87.8	98.6	62.502	0.029
48	4.5	18.70	0.0051	0.4923	0.738	99.7	99.2	62.509	0.052
34	4.5	18.67	0.0054	0.3885	1.140	94.2	99.4	62.512	0.035
60	4.5	18.67	0.0027	0.3785	1.064	190.2	99.4	62.513	0.035
22	4.5	18.67	0.0024	0.3638	0.885	216.5	99.4	62.516	0.042
84	4.5	18.69	0.0068	0.4535	1.402	74.6	99.3	62.519	0.028
86	4.5	18.63	0.0057	0.2374	1.349	88.8	99.6	62.524	0.029
58	4.5	18.71	0.0048	0.4906	1.204	105.5	99.2	62.546	0.033
30	4.5	18.85	0.0049	0.9480	1.043	104.5	98.5	62.555	0.039
15	4.5	18.77	0.0047	0.6691	1.537	107.7	98.9	62.556	0.027
41	4.5	18.69	0.0045	0.4059	1.698	113.2	99.4	62.557	0.024
62	4.5	18.76	0.0031	0.6351	1.190	163.5	99.0	62.561	0.034
63	4.5	18.75	0.0040	0.5922	1.375	126.9	99.1	62.563	0.029
21	4.5	18.73	0.0044	0.5220	1.249	115.6	99.2	62.570	0.034
18	4.5	18.74	0.0054	0.5593	1.357	94.3	99.1	62.577	0.029
89	4.5	18.64	0.0055	0.2137	2.039	92.5	99.7	62.584	0.020
68	4.5	18.74	0.0066	0.5386	1.298	77.4	99.2	62.603	0.030
76	4.5	18.72	0.0033	0.4339	1.266	155.8	99.3	62.613	0.031
45	4.5	18.73	0.0059	0.4501	1.904	87.1	99.3	62.647	0.022
47	4.5	18.80	0.0032	0.6781	0.680	158.6	98.9	62.653	0.057

APPENDIX 3

(continued)

ID	Power (watts)	$^{40}Ar/^{39}Ar$	$^{37}Ar/^{39}Ar$	$^{36}Ar/^{39}Ar$ (x 10^{-3})	$^{39}Ar_K$ (x10^{-15} mol)	K/Ca	$^{40}Ar^*$ (%)	Age (Ma)	±1σ (Ma)
H16-SJ-11, Detrital Sanidine, J=0.0018728±0.03%, IC=1.010695±0.0017517, NM-291D, Lab#=65815, Argus VI									
38	4.5	18.73	0.0056	0.4189	2.099	91.8	99.3	62.665	0.021
69	4.5	18.79	0.0048	0.2733	1.730	105.5	99.6	63.018	0.024
70	4.5	20.30	0.0062	0.2579	1.206	82.4	99.6	68.007	0.035
51	4.5	20.48	0.0034	0.8047	1.137	149.2	98.8	68.075	0.036
13	4.5	20.43	0.0059	0.6202	1.859	86.9	99.1	68.112	0.023
73	4.5	20.36	0.0030	0.3138	1.392	169.0	99.5	68.156	0.031
40	4.5	20.50	0.0040	0.4815	2.593	126.3	99.3	68.454	0.019
57	4.5	20.55	0.0048	0.6314	0.965	105.3	99.1	68.473	0.044
49	4.5	20.85	0.0019	0.3680	1.350	269.5	99.5	69.740	0.031
75	4.5	21.06	0.0079	0.6135	0.830	64.5	99.1	70.172	0.049
81	4.5	20.95	0.0044	0.2100	2.826	115.9	99.7	70.228	0.018
55	4.5	22.94	0.0029	3.425	0.422	177.9	95.6	73.66	0.10
02	4.5	32.49	0.0090	0.9612	1.675	56.6	99.1	107.18	0.18
42	4.5	68.99	0.0201	1.217	0.965	25.4	99.5	221.32	0.70
37	4.5	91.91	-0.0548	4.230	0.253	-	98.6	287.0	2.6
11	4.5	109.5	0.0248	1.153	0.802	20.6	99.7	340.4	1.3
10	4.5	130.2	-0.0010	1.411	0.958	-	99.7	398.4	1.5
01	4.5	205.1	0.0556	3.279	0.195	9.2	99.5	592.6	4.4
16	4.5	234.6	0.0151	6.574	0.532	33.8	99.2	662.1	3.9
20	4.5	475.0	0.0112	1.869	0.701	45.5	99.9	1163.8	9.0
50	4.5	501.0	0.0451	1.870	0.517	11.3	99.9	1210.4	9.7

REFERENCES

Archibald, J. D., Clemens, W. A., Gingerich, P. H., Krause, D. W., Lindsay, E. H., and Rose, K. D., 1987, First North American land mammal ages of the Cenozoic Era, *in* Woodburne, M. O., editor, Cenozoic mammals of North America: Berkeley, University of California Press, p. 24–76.

Atchley, S. C., Nordt, L. C., Dworkin, S. I., Cleveland, D. M., Mintz, J. S., and Harlow, R. H., 2013, Alluvial stacking pattern analysis and sequence stratigraphy: Concepts and case studies, *in* Driese, S. G., and Nordt, L. C., editors, New Frontiers in Paleopedology and Terrestrial Paleoclimatology: SEPM Special Publication, v. 104, p. 109–129.

Butler, R. F., and Lindsay, E. H., 1985, Mineralogy of Magnetic Minerals and Revised Magnetic Polarity Stratigraphy of Continental Sediments, San Juan Basin, New Mexico: The Journal of Geology, v. 93, n. 5, p. 535–554, https://doi.org/10.1086/628979

Butler, R. F., and Taylor, L. H., 1978, A middle Paleocene paleomagnetic pole from the Nacimiento Formation, San Juan Basin, New Mexico: Geology, v. 6, n. 8, p. 495–498, https://doi.org/10.1130/0091-7613(1978)6<495:AMPPPF>2.0.CO;2

Butler, R. F., Lindsay, E. H., Jacobs, L. L., and Johnson, N. M., 1977, Magnetiostratigraphy of the Cretaceous-Tertiary boundary in the San Juan Basin, New Mexico: Nature, v. 267, p. 318–323, https://doi.org/10.1038/267318a0

Cande, S. C., and Kent, D. V., 1992, A new geomagnetic polarity time scale for the Late Cretaceous and Cenozoic: Journal of Geophysical Research-Solid Earth, v. 97, n. B10, p. 13917–13951, https://doi.org/10.1029/92JB01202

Cather, S. M., 2004, Laramide orogeny in central and northern New Mexico and southern Colorado, *in* Mack, G. H., and Giles, K. A. editors, Geology of New Mexico: A geologic history: New Mexico Geological Society, Special Publication 11, p. 202–248.

Chapin, C. E., and Cather, S. M., 1981, Eocene tectonics and sedimentation in the Colorado Plateau-Rocky Mountain area, *in* Dickinson, W. R., and Payne, W. D., editors, Relations of Tectonics to Ore Deposits in the Southern Cordillera: Arizona Geological Society Digest, v. 14, p. 173–198.

Davis, A. J., Peppe, D. J., Atchley, S. C., Williamson, T. E., and Flynn, A. G., 2016, Climate and landscape reconstruction of the Arroyo Chijuillita Member of the Nacimiento Formation, San Juan Basin, New Mexico: Providing environmental context to early Paleocene mammal evolution: Palaeogeography, Palaeoclimatology, Palaeoecology, v. 463, p. 27–44, https://doi.org/10.1016/j.palaeo.2016.09.011

Dunlop, D. J., and Ozdemir, O., 1997, Rock Magnetism. Fundamentals and Frontiers: New York, Cambrdige University Press, 573 p., https://doi.org/10.1017/CBO9780511612794

Fisher, R. A., 1953, Dispersion of a sphere: Proceedings of the Royal Society of London, v. A217, n. 1130, p. 295–305, https://doi.org/10.1098/rspa.1953.0064

Granger, W., 1917, Notes on Paleocene and lower Eocene mammal horizons of northern New Mexico and southern Colorado: Bulletin of the American Museum of Natural History, v. 37, p. 821–830, http://hdl.handle.net/2246/1736

Guyodo, Y., LaPara, T. M., Anschutz, A. J., Penn, R. L., Banerjee, S. K., Geiss, C. E., and Zanner, W., 2006, Rock magnetic, chemical and bacterial community analysis of a modern soil from Nebraska: Earth and Planetary Science Letters, v. 251, n. 1–2, p. 168–178, https://doi.org/10.1016/j.epsl.2006.09.005

Hobbs, K. M., ms, 2016, Sedimentation, pedogenesis, and paleoclimate conditions in the Paleocene San Juan Basin, New Mexico, U.S.A.: Albuquerque, New Mexico, University of New Mexico, Ph. D. thesis, 160 p.

Kirschvink, J. L., 1980, The least-squares line and plane and the analysis of paleomagnetic data: Geophysical Journal International, v. 62, n. 3, p. 699–718, https://doi.org/10.1111/j.1365-246X.1980.tb02601.x

Kodama, K. P., 1997, A successful rock magnetic technique for correcting paleomagnetic inclination shallowing: Case study of the Nacimiento Formation, New Mexico: Journal of Geophysical Research-Solid Earth, v. 102, n. B3, p. 5193–5205, https://doi.org/10.1029/96JB03833

Kuiper, K. F., Deino, A., Hilgen, F. J., Krijgsman, W., Renne, P. R., and Wijbrans, J. R., 2008, Synchronizing the rock clocks of Earth history: Science, v. 320, n. 5875, p. 500–504, https://doi.org/10.1126/science.1154339

Lindsay, E. H., Jacobs, L. L., and Butler, R. F., 1978, Biostratigraphy and magnetostratigraphy of Paleocene terrestrial deposits, San Juan Basin, New Mexico: Geology, v. 6, n. 7, p. 425–429, https://doi.org/10.1130/0091-7613(1978)6<425:BAMOPT>2.0.CO;2

Lindsay, E. H., Butler, R. F., and Johnson, N. M., 1981, Magnetic polarity zonation and biostratigraphy of Late Cretaceous and Paleocene continental deposits, San Juan Basin, New Mexico: American Journal of Science, v. 281, n. 4, p. 390–435, https://doi.org/10.2475/ajs.281.4.390

Lofgren, D. L., Lillegraven, J. A., Clemens, W. A., Gingerich, P. D., and Williamson, T. E., 2004, Paleocene Biochronology: The Puercan Through Clarkforkian Land Mammal Ages, *in* Woodburne, M. O., editor, Late Cretaceous and Cenozoic Mammals of North America: New York, Columbia University Press, p. 43–105, https://doi.org/10.7312/wood13040-005

Lowrie, W., 1990, Identification of ferromagnetic minerals in a rock by coercivity and unblocking temperature properties: Geophysical Research Letters, v. 17, n. 2, p. 159–162, https://doi.org/10.1029/GL017i002p00159

Matthew, W. D., 1937, Paleocene faunas of the San Juan Basin, New Mexico: Transactions of the Philosophical Society, v. 30, p. 1–510, https://doi.org/10.2307/1005521

McFadden, P. L., and McElhinney, M. W., 1990, Classification of the reversal test in palaeomagnetism: Geophysical Journal International, v. 103, n. 3, p. 725–729, https://doi.org/10.1111/j.1365-246X.1990.tb05683.x

Min, K., Mundil, R., Renne, P. R., and Ludwig, K. R., 2000, A test for systematic errors in $^{40}Ar/^{39}Ar$ geochronology through comparison with U–Pb analysis of a 1.1 Ga rhyolite: Geochimica et Cosmochimica Acta, v. 64, n. 1, 73–98, https://doi.org/10.1016/S0016-7037(99)00204-5

Ogg, J. G., 2012, Geomagnetic polarity time scale, *in* Gradstein, F. M., Ogg, J. G., Schmitz, M. D., and Ogg, G. D., editors, The Geologic Time Scale: Oxford, United Kingdom, Elsevier, p. 85–113, https://doi.org/10.1016/B978-0-444-59425-9.00005-6

Osborn, H. F., 1929, The titanotheres of ancient Wyoming, Dakota, and Nebraska: U.S. Geological Survey, Monograph 55, p. 1–701.

Russell, D. E., 1967, Le Paleocene continental d'Amerique du Nord: Memoires du Museum National d'Histoire Naturelle (Nouvelle Series), Series C, v. 13, p. 1–32.

Sinclair, W. J., and Granger, W., 1914, Paleocene deposits of the San Juan Basin, New Mexico: American Museum of Natural History Bulletin, v. 33, p. 297–316.

Soil Survey Staff, 1999, Soil taxonomy: A basic system of soil classification for making and interpreting soil surveys. U.S. Department of Agriculture-NRCS Agriculture Handbook: Washington, U.S. Government Printing Office, 869 p.

Steiger, R. H., and Jäger, E., 1977, Subcommission on geochronology: Convention on the use of decay constants in geo- and cosmochronology: Earth and Planetary Science Letters, v. 36, n. 3, p. 359–362, https://doi.org/10.1016/0012-821X(77)90060-7

Szalay, F. S., and Lucas, S. G., 1996, The postcranial morphology of Paleocene *Chriacus* and *Mixodectes* and the phylogenetic relationships of archontan mammals: New Mexico Museum of Natural History and Science, v. 7, p. 1–47.

Taylor, J. R., 1982, An Introduction to Error Analysis: The Study of Uncertainties in Physical Measurements: Mill Valley, California, University Science Books, 270 p.

Taylor, L. H., ms, 1977, Geochronology of Torrejonian sediments, Nacimiento Formation, San Juan Basin, New Mexico: Tucson, Arizona, University of Arizona, M.S. thesis, 93 p.

Taylor, L. H., ms, 1984, Review of Torrejonian mammals from the San Juan Basin, New Mexico: Tucson, Arizona, University of Arizona, Ph. D. thesis, 553 p.

Taylor, L. H., and Butler, R. F., 1980, Magnetic-polarity stratigraphy of Torrejonian sediments, Nacimiento Formation, San Juan Basin, New Mexico: American Journal of Science, v. 280, n. 2, p. 97–115, https://doi.org/10.2475/ajs.280.2.97

Torsvik, T. H., Müller, R. D., Van der Voo, R., Steinberger, B., and Gaina, C., 2008, Global plate motion frames: Toward a unified model: Reviews of Geophysics, v. 46, n. 3, 44 p., https://doi.org/10.1029/2007RG000227

Tsentas, C., 1981, Mammalian biostratigraphy of the middle Paleocene (Torrejonian) strata of the San Juan Basin. Notes on Torreon Wash and the status of the *Pantolambda* and *Deltatherium* faunal "zones", *in* Lucas, S. G., Rigby, J. K., Jr., and Kues B. S., editors, Advances in San Juan Basin paleontology: Albuquerque, New Mexico, University of New Mexico Press, p. 262–292.

Watson, G. S., 1956, A test for randomness: Royal Astronomical Society Geophysical Supplement: Monthly Notices, v. 7, n. 4, p. 160–161, https://doi.org/10.1111/j.1365-246X.1956.tb05561.x

Weissmann, G. S., Hartley, A. J., Nichols, G. J., Scuderi, L. A., Olsen, M., Buehler, H., and Banteah, R., 2010,

Fluvial form in modern continental sedimentary basins: Distributive fluvial systems: Geology, v. 38, n. 1, p. 39–42, https://doi.org/10.1130/G30242.1

Williamson, T. E., 1996, The beginning of the age of mammals in the San Juan Basin, New Mexico: Biostratigraphy and evolution of Paleocene mammals of the Nacimiento Formation: New Mexico Museum of Natural History and Science Bulletin, v. 8, p. 1–141.

Williamson, T. E., and Lucas, S. G., 1992, Stratigraphy and mammalian biostratigraphy of the Paleocene Nacimiento Formation, southern San Juan Basin, New Mexico: New Mexico Geological Society Guidebook, 43rd Field Conference, San Juan Basin IV, p. 38–42.

Williamson, T. E., Nichols, D. J., and Weil, A., 2008, Paleocene palynomorph assemblages from the Nacimiento Formation, San Juan Basin, New Mexico, and their biostratigraphic significance: New Mexico Geology, v. 30, n. 1, p. 3–11.

Wilson, R. W., 1956, A new multituberculate from the Paleocene Torrejon fauna of New Mexico: Transactions of the Kansas Academy of Science, v. 59, n. 1, p. 76–84.

Wood, H. E., Chaney, R. W., Clark, J., Colbert, E. H., Jepsen, G. L., Reeside, J. B., Jr., and Stock, C., 1941, Nomenclature and correlation of the North American Continental Tertiary: Bulletin of the Geological Society of America, v. 52, n. 1, p. 1–48, https://doi.org/10.1130/GSAB-52-1